

1 **BioRT-Flux-PIHM v1.0: a watershed biogeochemical reactive transport**
2 **model**

3 Wei Zhi¹, Yuning Shi², Hang Wen¹, Leila Saberi³, Gene-Hua Crystal Ng³, ~~Li Li~~^{1*} Kayalvizhi
4 Sadayappan¹, Devon Kerins¹, Bryn Stewart¹, Li Li^{1*}

5 ¹ Department of Civil and Environmental Engineering, The Pennsylvania State University, State
6 College, PA 16802, USA

7 ² Department of Ecosystem Science and Management, The Pennsylvania State University, State
8 College, PA 16802, USA

9 ³ Department of Earth and Environmental Sciences, University of Minnesota, Twin Cities, MN
10 55455, USA

11 * Correspondence to lili@enr.psu.edu

Abstract

12

13 Watersheds are the fundamental Earth surface functioning unit that connects the land to
14 aquatic systems. ~~Existing~~Many watershed-scale models ~~typically have physics-~~
15 ~~based~~represent hydrological processes but often lack the representation of hydrology
16 ~~process but often lack mechanism-based~~, multi-component reactive transport processes
17 that are relevant to soil and aquatic biogeochemical reactions. The lack of mechanism-
18 based representation of reaction thermodynamics and kinetics. ~~This lack of~~ at the
19 watershed ~~reactive transport models~~scale has limited our ability to understand and predict
20 solute export and water quality, particularly under changing climate and anthropogenic
21 conditions. Here we present a recently developed BioRT-Flux-PIHM (~~BFP~~BioRT
22 hereafter) v1.0, a watershed-scale biogeochemical reactive transport model. Augmenting
23 the previously developed RT-Flux-PIHM that integrates land-surface interactions, surface
24 hydrology, and abiotic geochemical reactions (Bao et al., 2017, WRR), the new
25 development enables the simulation of 1) biotic processes including plant uptake, soil
26 respiration, and ~~microbe-microbially~~ mediated ~~biogeochemical~~ reactions ~~that are relevant~~
27 ~~to the~~such as carbon decomposition and nutrient transformation ~~of organic matter that~~
28 ~~involve carbon, nitrogen, and phosphorus~~; and 2) shallow and deep water partitioning to
29 represent surface, shallow groundwater, and deep groundwater interactions. The reactive
30 transport part of the code has been verified against the widely used reactive transport
31 code CrunchTope. BioRT-Flux-PIHM v1.0 has recently been applied to understand
32 reactive transport processes in multiple watersheds ~~across different~~under diverse
33 climate, vegetation, and ~~geology~~geological conditions. This paper briefly introduces the
34 governing equations and model structure ~~of the code with a focus on new model~~
35 developments. It also ~~demonstrates examples~~ showcases one hydrology example that
36 ~~simulates~~simulates shallow and deep water interactions, and two biogeochemical ~~reactive~~
37 ~~transport examples~~ relevant to nitrate and dissolved organic carbon (DOC). These
38 examples ~~were~~are illustrated in two simulation modes of varying complexity. One is the
39 spatially ~~implicit model~~lumped mode (i.e., two land cells connected by one river segment)
40 that focuses on processes and average behavior of a watershed. Another is ~~in a~~the
41 spatially ~~explicit~~distributed mode (i.e., hundreds of cells) that includes details of
42 topography, land cover, and soil property conditions. The spatially ~~explicit~~distributed

- 43 mode can be used to understand the impacts of spatial structure and identify hot spots of
44 biogeochemical reactions.

45 1. Introduction

46 Watersheds are the fundamental Earth surface units that receive and process
47 water, mass, and energy (~~Li, 2019~~); (Li, 2019; Li et al., 2020; Ranalli and Macalady,
48 2010; Hubbard et al., 2018; Seyfried et al., 2018). Watershed processes include land-
49 surface interactions that regulate evapotranspiration and discharge, and water
50 partitioning between shallow soil lateral flow going into streams versus downward flow
51 and recharge into the deeper subsurface (Edwards et al., 2015) (Figure 1). Complex
52 biogeochemical interactions also occur ~~between~~among soil, water, roots, and
53 ~~microb~~microbes, dictating ~~the~~CO₂ gas effluxes (e.g., CO₂) via soil respiration, export of
54 ~~soil~~solute products derived from chemical weathering and ~~biotransformation, and nutrient~~
55 ~~recycling~~ (Fatichi et al., 2019; van der Velde et al., 2010); biogeochemical transformation
56 (Fatichi et al., 2019; van der Velde et al., 2010; Grathwohl et al., 2013).

57 These hydrological and biogeochemical processes determine how Earthland
58 surface responds to external forcings such as hydroclimatic drivers and human
59 perturbations (~~van der Velde et al., 2014; Miller et al., 2020; Han et al., 2019; Steimke et~~
60 ~~al., 2018~~); (van der Velde et al., 2014; Miller et al., 2020; Han et al., 2019; Steimke et al.,
61 2018). Understanding these processes ~~remain~~remains challenging due to the complex
62 coupling of land surface processes, hydrology, and biogeochemical reactions (~~Kirchner,~~
63 ~~2003~~); (Kirchner, 2003). An example is the concentration-discharge (C-Q) relationships of
64 solutes at stream and river outlets. These relationships encode the integrated signature
65 of Earthland surface ~~response~~responses to changes in hydrological conditions. (Brooks
66 et al., 2015; Zhi et al., 2020; Zhi and Li, 2020). Similar C-Q relationships have been
67 observed for some solutes ~~across~~ watersheds under diverse geologygeological and
68 ~~climate~~climatic conditions (~~Godsey et al., 2009; Basu et al., 2010; Moatar et al.,~~
69 ~~2017; Zarnetske et al., 2018~~); (Godsey et al., 2009; Basu et al., 2010; Moatar et al.,
70 2017; Zarnetske et al., 2018; Godsey et al., 2019), whereas different solutes have shown
71 contrasting patterns in the same watershed (~~Miller et al., 2017; Herndon et al., 2015; Zhi~~
72 ~~et al., 2019; Musolff et al., 2015~~); (Miller et al., 2017; Herndon et al., 2015; Zhi et al.,
73 2019; Musolff et al., 2015). A general theory that can explain contrasting C-Q observations
74 (e.g., flushing vs. dilution behaviors) under diverse watershed characteristics and forcing

75 conditions remains elusive. The lack of understanding of mechanisms ~~that~~
76 ~~govern~~governing hydrological and biogeochemical interactions presents major
77 roadblocks for forecasting water quality ~~such that,~~ including water issues such as
78 eutrophication that persist worldwide.

79 One of the challenges ~~along these lines~~ answering questions relevant to water
80 quality and biogeochemical reactions is the lack of modeling tools that mechanistically
81 link hydrological and biogeochemical processes at the watershed scale. Model
82 development has been advancing ~~primarily~~ separately within the disciplinary boundaries
83 of hydrology and biogeochemistry (Li, 2019). ~~Hydrology models that~~ (Li, 2019). Hydrologic
84 models focus on solving for water storage and fluxes at the watershed scale and beyond
85 (Fatichi et al., 2016), and ~~reactive~~ (Fatichi et al., 2016). Reactive transport models (RTMs)
86 ~~that center on aqueous and solid concentration changes arising from~~ have traditionally
87 centered on transport and multi-component biogeochemical reactions typically in “~~closed~~”
88 groundwater systems ~~without much,~~ which often have limited interactions with “~~open~~”
89 ~~watersheds directly receiving precipitation and sunlight~~ (Steeffel et al., 2015; Li et al.,
90 2017b; Mayer et al., 2002; MacQuarrie and Mayer, 2005). This comes along with a history
91 ~~of hydrologists often trained as physicists studying fluid mechanics, and biogeochemists~~
92 ~~typically grow up as geologists, chemists, or~~ climate and other surficial watershed
93 processes (Steeffel et al., 2015; Li et al., 2017b; Mayer et al., 2002). Biogeochemical
94 reactions in shallow soils that are often driven by environmental ~~engineers~~ factors such as
95 soil temperature and moisture cannot be well simulated in these models.

96 ~~Recent works have shown some integration across these two lines. Examples~~
97 ~~include HSPF (Hydrological Simulation Program — FORTRAN) (Filoso et al.,~~
98 ~~2004; Laroche et al., 1996), SWAT (Soil & Water Assessment Tool) (Gassman et al.,~~
99 ~~2007; Lam et al., 2010; Moriasi et al., 2013; Neitsch et al., 2011), CATHY (Catchment~~
100 ~~Hydrology) (Gatel et al., 2019; Scudeler et al., 2016), PAWS (Process-based Adaptive~~
101 ~~Watershed Simulator) (Niu and Phanikumar, 2015; Qiu et al., 2019). These models have~~
102 ~~relatively crude representations of solute leaching out of element bulk mass as part of the~~
103 ~~solute export. These models do not represent kinetics and thermodynamics of multi-~~
104 ~~component biogeochemical reactions typically done in reactive transport models (RTMs).~~

105 In filling in this model development need, recently we developed the watershed reactive
106 transport code RT-Flux-PIHM that integrates kinetics and thermodynamics of multi-
107 component geochemical reactions with the land surface and hydrology model Flux-PIHM
108 (Bao et al., 2017). The geochemical reactions in RT-Flux-PIHM are abiotic, including
109 mineral dissolution and precipitation, aqueous and surface complexation, and ion
110 exchange reactions.

111 ——— This manuscript introduces BioRT-Flux-PIHM (BFPPrevious modeling
112 works has shown some integration across these two lines. For example, SWAT (Soil &
113 Water Assessment Tool) (Gassman et al., 2007;Lam et al., 2010;Moriassi et al.,
114 2013;Neitsch et al., 2011) includes a version that couples with the groundwater model
115 MODFLOW and simulates surface water and groundwater quality in RT3D (Bailey et al.,
116 2017; Ochoa et al., 2020). CATHY (Catchment Hydrology) includes processes of
117 pesticide decay (Gatel et al., 2019;Scudeler et al., 2016). Some other hydrological
118 models, including Hydrologiska Byråns Vattenbalansavdelning (HBV) and the
119 Hydrological Predictions for the Environment (HYPE), also have modules that simulate
120 processes relevant to nutrients and contaminants (Lindström et al., 2005;Lindström et al.,
121 2010). While many of these models can simulate reaction processes such leaching of
122 nutrients from agriculture lands (Lindström et al., 2005;Lindström et al., 2010;Bailey et
123 al., 2017), most of them do not explicitly solve the multi-component reactive transport
124 equations. In other words, they have relatively crude representations of solute leaching
125 out of element bulk mass as part of the solute export but do not represent kinetics and
126 thermodynamics of multi-component biogeochemical reactions typically included in
127 reactive transport models (RTMs). They also do not simulate processes such as chemical
128 weathering. As an example, nutrient leaching is often calculated based on empirical
129 equations without explicitly solving reactive transport equations. Reaction rates are often
130 represented using first-order decay (Gatel et al., 2019), assuming reaction rate constants
131 do not change with time and environmental conditions. However, biogeochemical
132 processes including carbon decomposition and nutrient cycling are highly variable in
133 space and time, depending on local environments such as substrate availability, soil
134 temperature, and soil moisture (Li et al., 2017a;Suseela et al., 2012;HARTLEY et al.,
135 2007). In filling in this model need, recently we augmented our watershed model RT-Flux-

136 PIHM (Bao et al., 2017) with new developments of microbially mediated reactions, which
137 allows us to model the interactions between biogeochemical reactions and environmental
138 factors that are driven by land surface and hydrological processes.

139 This manuscript introduces BioRT-Flux-PIHM (BioRT hereafter) v1.0, augmented
140 based on RT-Flux-PIHM with two new additions. One is the capability of simulating biotic
141 processes including plant uptake of nutrients, soil respiration, and microbe-microbially
142 mediated reactions in the soil. ~~These soil processes~~ Examples include the transformation
143 of fresh and old organic matter, for example, soil respiration that produces CO₂ and
144 carbon decomposition that generates dissolved organic carbon (DOC), and other nutrient
145 cyclings transformation processes such as nitrification and denitrification. The other is the
146 introduction of an optional deeper layer below the shallow soil that enables the
147 simulation of interactions of deep water and shallow soil water flow (Figure 1). Here the
148 deep water is loosely defined as the water beyond the soil zone, typically in less
149 weathered, fractured subsurface that harbors ~~the~~ relatively old and slow-moving
150 groundwater contributing to streams. This contrasts ~~the~~with shallow water in highly
151 permeable soils. Mounting evidence in recent years has shown that ~~the~~ deeper water
152 beyond the shallow soil interacts with streams, bringsintroduces water with distinct
153 chemistry, sustains base flow in dry times, and buffers climate variability (~~Gurdak,~~
154 ~~2017;Green, 2016;Taylor et al., 2013;Condon et al., 2013;Anyah et al., 2008;Maxwell et~~
155 ~~al., 2011;Gleeson et al., 2015).~~ They are therefore(Gurdak, 2017;Green, 2016;Taylor et
156 al., 2013;Condon et al., 2013;Anyah et al., 2008;Maxwell et al., 2011;Gleeson et al.,
157 2015). Stream chemistry often reflects the distinct chemistry from the shallow soil and
158 deeper groundwater zones, i.e., the so called Shallow and Deep Hypothesis (Zhi et al.,
159 2019;Zhi and Li, 2020). Deeper groundwater is thus a fundamental component of the
160 hydrologic cycle and water budget. The groundwater-surface water interactions can also
161 modulate land-atmospheric energy exchanges and soil moisture dynamics- (~~Keune et al.,~~
162 ~~2016;Martínez-de la Torre and Miguez-Macho, 2019).~~ Including the deep water
163 component ~~therefore~~thus enables the simulation of such interactions and the dynamics
164 of water quality.

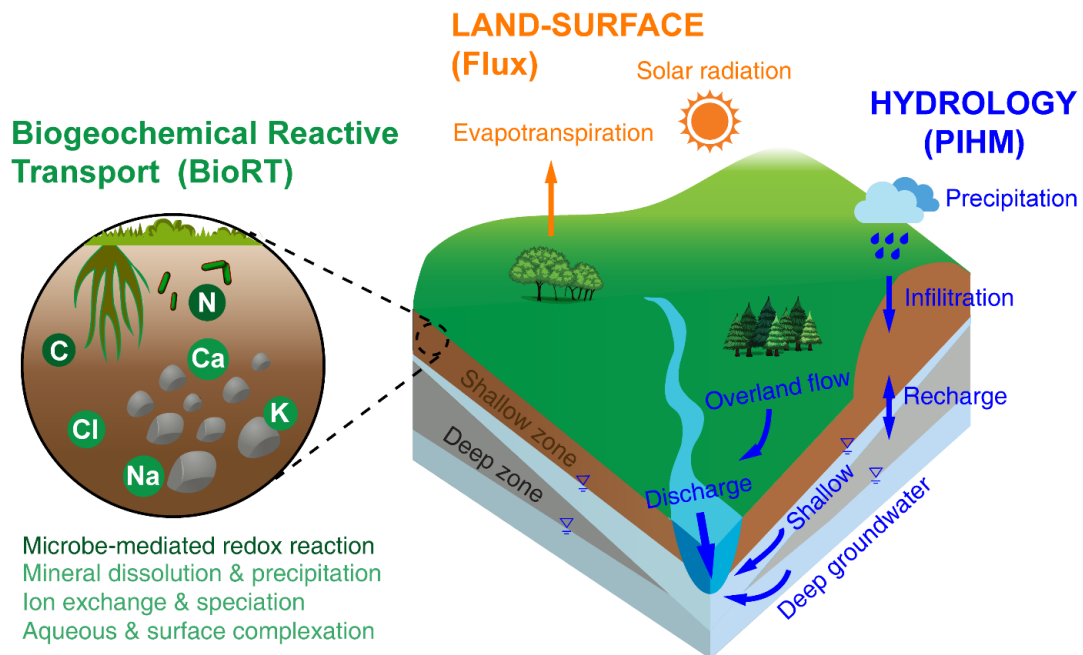
165 This paper introduces new developments in the governing equations, BioRT model
166 structure and capabilities of BFP. The biogeochemical reactive transport. The code has
167 been verified against the widely used reactive transport code CrunchTope (Supporting
168 Information), SI. This paper briefly overviews water and energy related processes
169 incorporated in the model. Readers are referred to previous publications for more details
170 of processes such as evapotranspiration (ET), hydrological flow, and abiotic reactions
171 (Shi et al., 2013; Bao et al., 2017; Li et al., 2017a; Qu and Duffy, 2007). We showcase the
172 model using two examples three examples that illustrate the new model capabilities and
173 the simulation of varying complexity: one biogeochemical reactions. The first hydrological
174 example shows the surface water and groundwater interactions. This second example
175 focuses on nitrate processes run transformation and transport in a spatially implicit lumped
176 mode; another on. The third example examines the production and transport export of
177 dissolved organic carbon (DOC) in a spatially explicit mode with the representation of
178 spatial details. The source code and the examples shown here are hosted in on the GitHub
179 page GitHub website (<https://github.com/PSUmodeling/BioRT-Flux-PIHM>).

181 **2. Model description overview**

182 BioRT-Flux-PIHM integrates different processes in three modules (Figure 1). The
183 Flux module is for land surface interaction processes including surface energy balance,
184 solar radiation, and evapotranspiration (ET) (Shi et al., 2013). The hydrology module
185 PIHM simulates water processes including precipitation, interception, infiltration,
186 recharge, surface runoff, subsurface lateral flow, and deep water flow (Qu and Duffy,
187 2007). The BioRT module is for multi-component biogeochemical reactive transport
188 processes including microbe-mediated redox reactions (e.g., carbon decomposition and
189 nutrient transformation), ion exchange, aqueous and surface complexation, and mineral
190 dissolution and precipitation.

191
192 BioRT-Flux-PIHM integrates three modules (Figure 1). The Flux module is for land-
193 surface processes including surface energy balance, solar radiation, and ET (Shi et al.,
194 2013). The hydrology module PIHM simulates water processes including precipitation,

195 interception, infiltration, recharge, surface runoff, subsurface lateral flow, and deep water
 196 flow (Qu and Duffy, 2007). The BioRT module simulates solute transport, bio-relevant
 197 processes such as plant uptake of nutrients from water, and multi-component reactions.
 198 The reaction processes can include soil respiration, microbially mediated redox reactions
 199 (e.g., soil respiration, carbon decomposition and nutrient transformation), ion exchange,
 200 aqueous and surface complexation, and mineral dissolution and precipitation. Note that
 201 geochemical reactions in our previous RT-Flux-PIHM are abiotic (Bao et al., 2017),
 202 including mineral dissolution and precipitation, aqueous and surface complexation, and
 203 ion exchange reactions.



204

205 **Figure 1.** A conceptual diagram for processes at the watershed scale. This includes land surface
 206 land interactions such as energy balance, solar radiation, evapotranspiration (e.g., evaporation,
 207 transpiration, and snow sublimation); hydrological processes partitioning water between surface
 208 runoff, shallow soil water lateral flow, and deeper water entering the stream; and soil. Soil
 209 biogeochemical reactions includinginclude abiotic reactions (e.g., mineral dissolution and
 210 precipitation, ion exchange, surface complexations), and biotic processes such as soil respiration,
 211 plant uptake of nutrients, and other microbe-mediated reactions such as the transformation of
 212 carbon and nitrogen. These processes are represented in three modules: theThe Flux module for
 213 land-surface interaction-processesinteractions, the PIHM module for catchment hydrology
 214 processes, and the recently augmented BioRT module for soil biogeochemical reaction
 215 processesreactions. Conceptually the shallow water zone includesis the shallow subsurface such
 216 as soil and weathered zone that are more conducive to water flow (e.g., soil lateral flow or

217 interflow). The deep zone refers to the less weathered, ~~fractured~~ zone that often harbors the
218 relatively old and slow flowing ~~water that contributes to stream flow.~~groundwater. Reactions can
219 occur in both shallow and deep zones. For the BioRT, the light and dark greens refer to abiotic
220 and biological reactions, respectively.

221

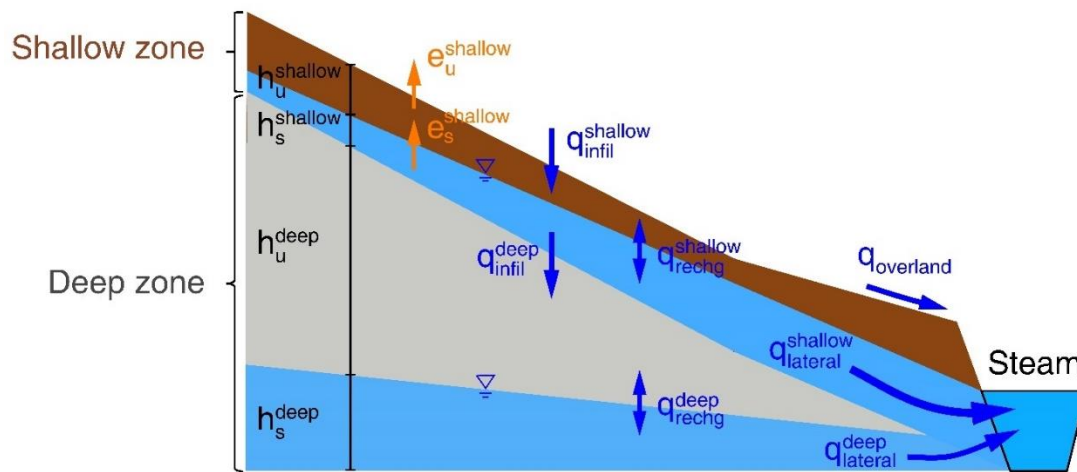
222 The land surface and hydrology modules ~~are coupled to~~ solve for soil temperature
223 and water storage, from which water fluxes can be quantified for surface runoff, shallow
224 and deep water fluxes. The BioRT module uses the calculated soil temperature, water
225 storage, and water fluxes to simulate advection, diffusion ~~—/—~~/dispersion, and
226 biogeochemical reactions in both shallow and deep zones. (see governing equations in
227 later sections). The reactions can be ~~kinetics-~~kinetically controlled (e.g., microbial redox
228 reaction) or ~~thermodynamically—equilibrium-~~controlled (e.g., ion exchange, surface
229 complexation (sorption), and aqueous complexation). Users can define the types of
230 reactions to be included and the form of reaction kinetics in ~~the~~ input files. The output of
231 BioRT includes the spatial distribution and time series of aqueous and solid
232 concentrations ~~in shallow and deep zones and in stream water, from which we can also~~
233 infer reaction rates.

234 The simulation domain ~~can be discretized into~~ is structured as prismatic grids
235 based on topography. Each grid is partitioned into surface and shallow and deep
236 subsurface layers. The surface layer calculates water flow above ground (surface runoff).
237 The shallow subsurface zone is loosely defined as the highly permeable subsurface that
238 ~~are most conductive to water flow,~~ is contrasting to the deep zone that is broadly defined
239 as the lower permeability zone beyond the shallow zone. In many places, this shallow
240 zone is the soil zone that is most conductive to water flow (e.g., soil lateral flow) and is
241 ~~very-~~responsive to hydroclimatic ~~forcing~~forcings. The deep subsurface zone is the less
242 weathered, ~~fractured~~ layer that harbors the relatively ~~old~~older and ~~slow~~lower flowing
243 ground water that contributes to stream flow. Note that these definitions differ from those
244 in the hydrology community, which often ~~refer~~refers to the shallow soil water flow or
245 lumped shallow soil as groundwater, in a way that distinguishes it from the surface runoff
246 (Winter et al., 1998; Dingman, 2015; Todd and Mays, 2005). As illustrated in Figure 1, both
247 shallow (Winter et al., 1998; Dingman, 2015; Todd and Mays, 2005). These shallow and

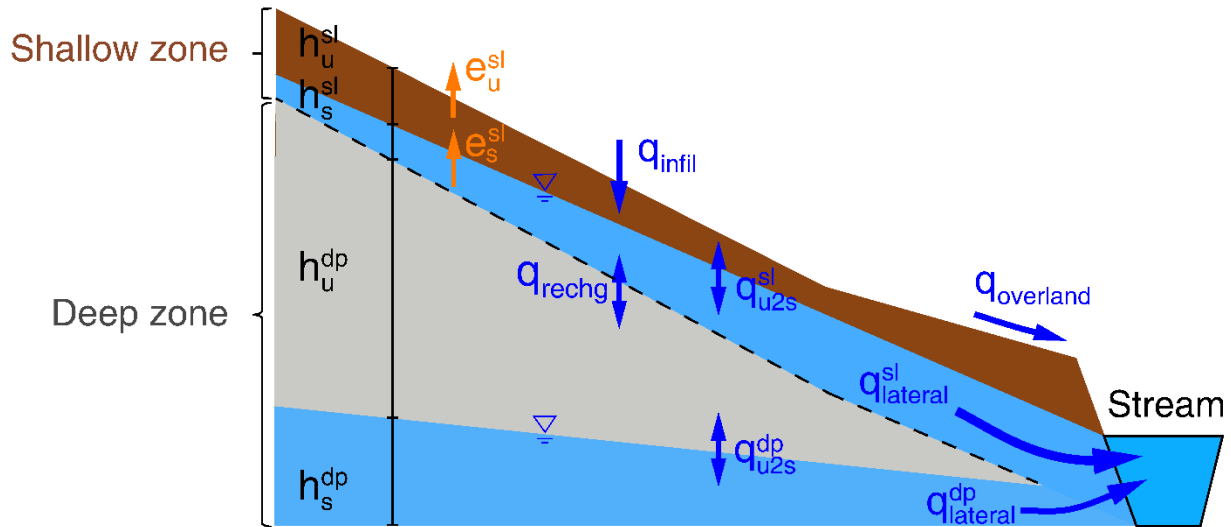
248 deep zone waters often have unsaturated distinct solid and saturated layers, enabling the
 249 simulation water chemistry, and are dominant at different time of the “two water tables”
 250 (Brantley et al., 2017). These transient water tables year, as have been observed in and
 251 inferred in many catchments and watersheds (Brantley et al., 2018; Zhi et al., 2019; Zhi
 252 and Li, 2020; Li et al., 2020; Sullivan et al., 2016). Despite the model complexity, the model
 253 is flexible for taking inputs from online data portals or local measurements and it can
 254 accommodate low data availability (see the following section of Shale Hills, Garner Run,
 255 and Cole Farm (Li et al., 2018; Brantley et al., 2018).5 for data need and domain setup).
 256 The model is developed as a research tool to understand coupled watershed processes
 257 rather than as a policy model to guide management.

258

259 **3. Governing equations and processes**



260



261
 262 **Figure 2.** Hillslope view of the shallow and deep zones and relevant water flows. The symbol of
 263 “h”, “e”, and “q” denotes water head, storage [m], evapotranspiration, [m/s], and water flow, [m/s],
 264 respectively. The superscript letter “sl” and “dp” refer to shallow and deep zone, respectively. The
 265 subscript letter letters “u” and “s” refers refer to unsaturated and saturated layer, respectively.
 266 Detailed equations are listed in the following sections. The terms “infil”, “u2s”, and “recharge” refer
 267 to infiltration, unsaturated to saturated zones, and recharge.

268
 269 **3.1 The water Water equations in**

270 The original Flux-PIHM simulates surface runoff and a lumped subsurface flux into
 271 streams without distinguishing shallow and deep soil water flow and deeper groundwater
 272 flow. In working with stream water chemistry data, we realized that a lumped subsurface
 273 flow cannot describe the dynamics of stream chemistry, as the shallow soil water and
 274 deeper groundwater have distinct chemistry and are dominant at different times of the
 275 year (Zhi et al., 2019; Zhi and Li, 2020). We therefore added an optional deeper
 276 groundwater zone in the code to simulate the deeper water that interacts with streams.
 277 Each prismatic element now has three zones in the vertical direction: surface (or above
 278 ground), shallow and deep zones in the subsurface.

279 As shown in Figure 2, in each prismatic element i , the shallow zone hasincludes
 280 unsaturated and saturated water storages. The unsaturated zone receives water from
 281 the surface via infiltration and interactions between the two storagesonly flows vertically
 282 to the saturated zone. The saturated zone flows both vertically to the deep zone

283 (recharge) and laterally to neighboring grids j or the stream (lateral). The code solves the
 284 following equations for the shallow zone:

$$285 \theta_i^{shallow} \frac{dh_u^{shallow}}{dt} = q_{infil}^{shallow} - q_{rechg}^{shallow} - e_u^{shallow} \quad (1)$$

$$286 \theta_s^{shallow} \frac{dh_s^{shallow}}{dt} = q_{rechg}^{shallow} - q_{infil}^{deep} - e_s^{shallow} + \sum_{ij}^{\pm} q_{lateral-ij}^{shallow} \quad (2)$$

$$287 \theta_i^{sl} \frac{dh_{i,u}^{sl}}{dt} = q_{i,infil} - q_{i,u2s}^{sl} - e_{i,u}^{sl} \quad (1)$$

$$288 \theta_i^{sl} \frac{dh_{i,s}^{sl}}{dt} = q_{i,u2s}^{sl} - q_{i,rechg} - e_{i,s}^{sl} + \sum_1^{N_{ij}} q_{ij}^{sl} \quad (2)$$

289 Where $\theta_u^{shallow}$ and $\theta_s^{shallow} \theta_i^{sl}$ [m³ pore space/m³ total volume] is the shallow zone
 290 porosity in the element i ; $h_{i,u}^{sl}$ and $h_{i,s}^{sl}$ [m] are the unsaturated and saturated water storage
 291 in the shallow zone, respectively; $\theta^{shallow}$ is the shallow zone porosity; $q_{infil}^{shallow}$ and q_{infil}^{deep} .
 292 Note that the storages h here are the shallow and deep essentially the height of soil
 293 column with equivalent saturated water, not the height of the pure water (100% volume)
 294 column. That is why porosity is in the equation. For saturation zones, this height is needed
 295 to quantify the depths of water tables and determines the direction of water flow between
 296 neighboring grids. The $q_{i,infil}$ [m/s] is the infiltration rate from the surface to the shallow
 297 zone and from the shallow to the deep zone, respectively; $q_{rechg}^{shallow}$ and q_{rechg}^{deep} are the
 298 recharge; $q_{i,u2s}^{sl}$ [m/s] is the vertical flow from the unsaturated layer to the saturated layer
 299 in the shallow and deep zones, respectively; $e_u^{shallow}$ zone; $q_{i,rechg}$ [m/s] is the recharge
 300 rate from the shallow zone to the deep zone; $e_{i,u}^{sl}$ and $e_s^{shallow} e_{i,s}^{sl}$ [m/s] are shallow
 301 evapotranspiration (ET) from the unsaturated and saturated layer (Shi, 2012); in the
 302 shallow zone, respectively; $q_{lateral-ij}^{shallow}$ is the shallow normalized q_{ij}^{sl} [m/s] are the lateral
 303 fluxflows in the shallow saturated layer from between the element i and its neighbor
 304 element j (≤ 3); N_{ij} (≤ 3) is the number of neighbor elements j . For a prismatic element
 305 i , a boundary cell could have one or two neighbors; a non-boundary cell has three
 306 neighbors. The ET is calculated by the Penman potential evaporation scheme and

detailed equations can be found in Shi (2012). A similar set of water equations for the deep zone are in the SI (Eqn. S1 and S2).

Infiltration and recharge vertical fluxes from the unsaturated to the saturated layer in the shallow zone for the elements i are calculated using are based on the Richards equation, in which hydraulic water head H (i.e., the summation of water storage h and elevation head z) and hydraulic conductivity K are used to determine the fluxes in each element i :

$$q_{infil}^{shallow} = AK_{infil}^{shallow} \frac{H_{sur} - H_{\#}^{shallow}}{D_{inf}} \quad (3)$$

$$q_{rechg}^{shallow} = AK_{effv}^{shallow} \frac{H_{\#}^{shallow} - H_s^{shallow}}{0.5D_{shallow}} \quad (4)$$

$$q_{i,inf} = K_{i,inf} \frac{H_{i,sur} - H_{i,u}^{sl}}{d_{i,inf}} \quad (3)$$

$$q_{i,u2s}^{sl} = K_{i,v}^{sl} \frac{H_{i,u}^{sl} - H_{i,s}^{sl}}{0.5d_i^{sl}} \quad (4)$$

Where A is the element area in the vertical direction; $D_{inf}d_{i,inf}$ and $D_{shallow}d_i^{sl}$ [m] are the thickness of infiltration (0.1 m) layer and shallow layer zone depth for the elements i , respectively; $K_{infil}^{shallow}$ and $K_{effv}^{shallow}$ are the infiltration and effective $K_{i,inf}$ [m/s] is the hydraulic conductivity in the vertical direction in the shallow zone, respectively; of the infiltration layer, the top 0.1 m of the subsurface and is considered to have different conductivity from the rest of subsurface; $K_{i,v}^{sl}$ [m/s] is the hydraulic conductivity in the vertical direction (i.e., weighted average of macropore $K_{i,macv}$ and soil matrix $K_{i,satv}$, Eqn. S7); $H_{sur}H_{i,sur}$ [m] is the surface hydraulic water head ($= h_{sur}h_{i,sur} + z_{sur}z_{i,sur}$); $H_{\#}^{shallow}H_{i,u}^{sl}$ and $H_s^{shallow}H_{i,s}^{sl}$ [m] are the shallow hydraulic water headheads in the unsaturated and saturated layer, respectively. ShallowThe lateral flow in the shallow saturated layer is calculated using Darcy's law:

$$q_{lateral-t}^{shallow} = A_{tj}K_{effH-t}^{shallow} \frac{(H_s^{shallow})_t - (H_s^{shallow})_f}{D_{tj}} \quad (5)$$

330

$$q_{ij}^{sl} = K_{ij}^{sl} \frac{H_{i,s}^{sl} - H_{j,s}^{sl}}{d_{ij}} \quad (5)$$

331

332

333

334

335

336

Where A_{ij} is the projection area of the saturated layer between elements i and j ; D_{ij} is the d_{ij} [m] is the distance between the centers of elements i and j ; $K_{effH-ij}^{shallow} K_{ij}^{sl}$ [m/s] is the harmonic mean of shallow effective-hydraulic conductivity in the horizontal direction ($K_{effH}^{shallow}$) between elements i ($K_{i,H}^{sl}$) and j ($K_{j,H}^{sl}$). The interaction between the shallow saturated zone and stream channel also follows the Eq. (Eqn. 5), where, except that the adjacent head is replaced by the level of the channel water.

337

338

339

Similar to the shallow zone, hydrological equations in the deep zone in each element i can have unsaturated and saturated storages, with unsaturated-saturated flow within i ; are detailed in the SI (Eqn. S1 – S8).

340

$$\theta^{deep} \frac{dh_u^{deep}}{dt} = q_{infil}^{deep} - q_{rechg}^{deep} \quad (6)$$

341

$$\theta^{deep} \frac{dh_s^{deep}}{dt} = q_{rechg}^{deep} + \sum_j^{\pm} q_{lateral-ij}^{deep} \quad (7)$$

342

343

344

345

Where h_u^{deep} and h_s^{deep} are the unsaturated and saturated storages in the deep zone, respectively; θ^{deep} is the deep zone porosity; q_{rechg}^{deep} is the deep recharge flux from the unsaturated layer to the saturated layer; $q_{lateral-ij}^{deep}$ is the deep normalized lateral flux from element i to its neighbor j (≤ 3).

346

Deep lateral flow is calculated using Darcy's law:

347

$$q_{lateral-ij}^{deep} = A_{ij} K_{effH-ij}^{deep} \frac{(H_s^{deep})_i - (H_s^{deep})_j}{D_{ij}} \quad (8)$$

348

349

350

Where H_s^{deep} is the deep hydraulic water head; $K_{effH-ij}^{deep}$ is the harmonic mean of the deep effective hydraulic conductivity in the horizontal direction (K_{effH}^{deep}) between elements i and j .

351

352

Deep infiltration and recharge fluxes are similarly calculated using the Richards equation as in the shallow zone:

$$q_{infil}^{deep} = AK_{infil}^{deep} \frac{H_s^{shallow} - H_u^{deep}}{0.5 [H_s^{shallow} + (D^{deep} - H_s^{deep})]} \quad (9)$$

$$q_{rechg}^{deep} = AK_{effV}^{deep} \frac{H_u^{deep} - H_s^{deep}}{0.5 D^{deep}} \quad (10)$$

Where K_{infil}^{deep} is the hydraulic conductivity of infiltration from the shallow zone to the deep zone; D^{deep} is the thickness of the deep zone; K_{effV}^{deep} is the effective hydraulic conductivity in the vertical direction of the deep zone.

The deep groundwater can also come from regional groundwater aquifers, which can set up as an influx from the boundary of the domain. Deep groundwater interacts with river channel via the shallow zone. When the level of deep groundwater is higher than the depth to the deep zone, i.e., the shallow transient groundwater and the deep groundwater are connected, the deep groundwater can flow into the transient saturated layer in the shallow zone:

$$q_{infil}^{deep} = -AK_{satV}^{deep} \quad (11)$$

Where K_{satV}^{deep} is the saturated hydraulic conductivity in the vertical direction of the deep zone.

Macropores. Macropores, including roots and soil cracks are omnipresent in soils. Macropore flows can be simulated in the model to account for rapid water flows in the shallow zone (Shi et al., 2013). Macropore properties include depth (D_{mac}) and macropore vertical and horizontal area fraction (f_{macV} and f_{macH}), and vertical and horizontal hydraulic conductivity ($K_{macV}^{shallow}$ and $K_{macH}^{shallow}$). The macropore depth differs from the rooting depth, which specifies the maximum depth of transpiration. By default $K_{macV}^{shallow}$ and $K_{macH}^{shallow}$ are 100 and 1,000 times of the infiltration hydraulic conductivity ($K_{infil}^{shallow}$) and shallow horizontal hydraulic conductivity ($K_{satH}^{shallow}$), respectively, and can be changed during calibration. Taking both soil and macropore properties into account, the effective hydraulic conductivity of the subsurface is calculated as the weighted average of the macropore and the shallow soil matrix within the macropore depth (Eq. (12) and (13)).

$$K_{effV}^{shallow} = f_{macH} K_{macV}^{shallow} + (1 - f_{macH}) K_{satV}^{shallow} \quad (12)$$

$$K_{effH}^{shallow} = f_{macv} K_{mach}^{shallow} + (1 - f_{macv}) K_{satH}^{shallow} \quad (13)$$

3.2 Biogeochemical reactive transport equations

The governing advection dispersion reaction (ADR) equation for an arbitrary solute m in grid i is as follows (Bao et al., 2017), i.e., the change of solute mass (i.e., the left term in Eqn. 6) is driven by dispersive transport, advective transport, and reactions (i.e., the 1st, 2nd, and 3rd right-hand side terms, respectively):

$$V_i \frac{d(S_{w,i} \theta_i C_{m,i})}{dt} = \sum_{j=N_{i,x}}^{N_{i,x}} \left(A_{ij} D_{ij} \frac{C_{m,j} - C_{m,i}}{l_{ij}} - q_{ij} C_{m,j} \right) + R_{m,i} \quad (14) \frac{d(S_{w,i} \theta_i C_{m,i})}{dt}$$

$$= \sum_1^{N_{ij}} \left(A_{ij} D_{ij} \frac{C_{m,j} - C_{m,i}}{d_{ij}} - q_{ij} A_{ij} C_{m,j} \right) + R_{m,i}, \quad m = 1, \dots, nm \quad (6)$$

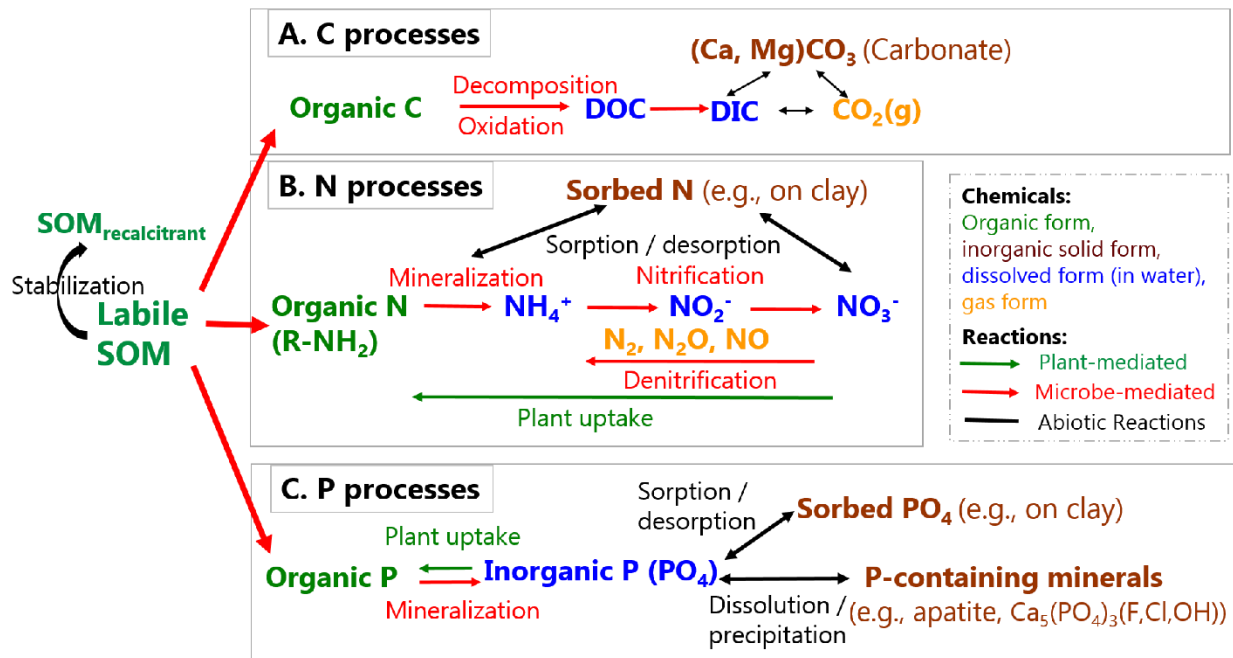
Where V_i is the [m³ total volume of grid i (solid + liquid) is the total volume], m³ of element i ; $S_{w,i}$ [m³ water/m³ pore space] is soil water saturation, m³ water/m³ pore space; θ_i is porosity, [m³ pore space/m³ total volume] is porosity; $C_{m,i}$ [mol/m³ water] is the aqueous concentration of species m , mol/m³ water; N_{ij} is the number of fluxes from neighbor element j for element i ; $N_{i,x}$ is the index of elements sharing surfaces; the value of xN_{ij} is 2 for the unsaturated zone (infiltration, recharge) with only vertical flows and 45 for the saturated zone (recharge plus with flux from (or to) the unsaturated zone, from (or to) the deeper zone, and fluxes between i and three neighbor elements j in lateral flow directions), respectively for non-boundary grids; A_{ij} [m²] is the interfacegrid area (m²) shared by i and its neighbor grid j ; D_{ij} [m²/s] is the combinedhydrodynamic dispersion/ coefficient (i.e., sum of mechanical dispersion and effective diffusion coefficient) (m²/s) normal to the shared surface A_{ij} ; $l_{ij}d_{ij}$ [m] is the distance between the center of i and its neighbor elements j ; q_{ij} [m/s] is the flow rate across A_{ij} , m³/s; $R_{m,i}$ [mol/s] is the total rate of kinetically controlled reactions in element i that involve species m , mol/s; nm is the total number of independent primary species to be solved for reactive transport equations.

— Various types of

405 3.3 Biogeochemical processes and reaction kinetics

406 3.3.1 Biogeochemical processes

407 Here we discuss some representative biogeochemical processes that involve
408 plants and microbes that can be included in BioRT. BioRT differs from general water
409 quality models that often primarily target a few contaminants (e.g., N, P, metals). The
410 framework of the subsurface (Fatichi et al., 2019).code is flexible and the users can define
411 their reactions and solutes of interests in the input files. For abiotic reactions such as
412 mineral dissolution and surface complexation or ion exchange, readers are referred to an
413 earlier paper (Bao et al. (2017)). Generally speaking, shallow soils compared to deep soils
414 contain more weathered materials and soil organic matters (SOM) including roots,
415 leaves, and microbe. In contrast, deeper zones are less weathered and contain much
416 less organic matter. SOM can decompose microbes. SOM can be decomposed partially
417 into organic molecules that dissolve in water (Wieder et al., 2015),(Wieder et al., 2015),
418 i.e., DOC, or oxidize it can be oxidized completely into CO₂ that is released back to the
419 atmosphere as a gas or (Davidson, 2006) or surface water in the form of dissolved
420 inorganic carbon (DIC). With coexisting divalent cations (e.g., Ca, Mg), DIC can also often
421 precipitate and become carbonate minerals. Hence soil C decomposition can release CO₂
422 back into the atmosphere and changes CO₂ level (Davidson, 2006), or releases DOC and
423 DOM to surface water. These processes occur in soils and also as dissolved carbon
424 transport laterally to streams. (e.g., CaCO₃).



425
 426 **Figure 3.** Various types of biotic and abiotic reactions relevant to the transformation of soil organic
 427 matter (SOM). It can become stabilized through sorption on clay and separation from reactants.
 428 It can also decompose into inorganic forms, transitioning between different phases (adopted from
 429 Li (2019)). Biotic and abiotic reactions relevant to the transformation of soil organic matter (SOM).
 430 It can become stabilized through sorption on clay and separation from reactants. Labile OM can
 431 decompose into inorganic forms, releasing C, N, and P that further transform between different
 432 forms (adopted from Li (2019), permission with Mineralogical Society of America).

433
 434 Shown in Figure 3, SOMOM decomposition releases organic nitrogen (R-NH₂),
 435 which can further react to become ammonia, NH₄⁺, and other nitrogen forms in-between
 436 (N₂, N₂O, NO, N₂O₃-(NO₂)₂, NO₂). Some of the gaseous forms emit (Figure 3). The
 437 gases can be emitted back to the atmosphere (Saha et al., 2017; Maavara et al.,
 438 2018). (Saha et al., 2017; Maavara et al., 2018). Denitrification requires anoxic conditions
 439 and does not occur as much occurs less commonly in shallow soils owing to the pervasive
 440 presence of O₂ (Sebestyen et al., 2019); (Sebestyen et al., 2019); it can become prevalent
 441 however important under extremely wet conditions and in O₂-depleted groundwater
 442 systems. In soils, Phosphorous (P) can be in an organic form (e.g., leaves), sorbed (on
 443 fine soil particles), dissolved in water, or in solid forms as P-containing minerals (Figure
 444 3). The transformation between different forms. Transformation of nutrients occurs
 445 through various bio-mediated or abiotic reactions. The most abundant A representative P-
 446 containing mineral in the Earth's crust is apatite Ca₅(PO₄)₃(F, Cl, OH). Once liberated via

447 rock dissolution, P is mostly biologically assimilated and locked in organisms. It is barely
448 soluble so it binds organic forms. These organic forms have very low solubility, allowing
449 them to bind on and transports be transported together with soil particles in the form of
450 orthophosphate or pyro-diphosphate. Overall, these reactions are a combination of biotic
451 and abiotic reactions.

452 ~~BioRT can simulate biotic reactions including microbe-mediated reactions~~

453 3.3.2 Reaction kinetics in natural soils

454 Rate dependence on temperature and soil moisture. Reactions such as soil
455 respiration and plant uptake, in addition to the abiotic reactions such as mineral
456 dissolution and surface complexation or ion exchange that have been introduced by Bao
457 et al. (2017). Here we focus on the discussion of a few representative microbe-mediated
458 reactions.

459
460 ~~Microbe-mediated reaction kinetics.~~ SOM is often conceptualized and modeled as
461 pools with different decomposition rates and turnover times (Ostle et al., 2009; Thornton
462 et al., 2009). An extensively used three-pool model includes a readily degradable (labile)
463 pool with residence times less than five years; a slowly degrading pool with residence
464 times of decades; and a relatively stable pool, with residence times between 10^3 – 10^5
465 years (Trumbore et al., 1995; Trumbore, 1993; Marin-Spiotta et al., 2009). The kinetics of
466 microbe-mediated reactions can be described by the general dual Monod rate law,
467 reflecting the need for both electron donor and acceptor in these reactions (Monod, 1949):

$$468 \quad r = \mu_{max} C_{C_5H_7O_2N} \frac{C_D}{K_{m,D} + C_D} \frac{C_A}{K_{m,A} + C_A} \quad (15)$$

469 Here μ_{max} is the rate constant (mol/time/microbe cell), $C_{C_5H_7O_2N}$ is the concentration of
470 microorganisms (microbe cells/L³), C_D and C_A are the concentrations of electron donor
471 and acceptor (mol/L³), respectively. The $K_{m,D}$ and $K_{m,A}$ are the half-saturation coefficients
472 of the electron donor and acceptors (mol/m³), respectively; they are the concentrations at
473 which half of the maximum rates are reached for the electron donor and acceptor,
474 respectively. If an electron donor or acceptor is not limiting, it means that $C_D \gg K_{m,D}$ or

475 $C_A \gg K_{m,A}$, so that the term $\frac{C_D}{K_{m,D} + C_D}$ or $\frac{C_A}{K_{m,A} + C_A}$ is essentially 1, lending to a rate that only
 476 depends typically depend on the abundance of microorganisms or one of the chemicals.

477 In natural subsurface where multiple electron acceptors coexist, the
 478 biogeochemical redox ladder dictates the sequence of redox reactions. That is, aerobic
 479 oxidation occurs before denitrification, which in turn occurs before iron reduction.
 480 Inhibition terms are used to account for the sequence of redox reactions as follows:

$$481 \quad r = \mu_{max} C_{C_5H_7O_2N} \frac{C_D}{K_{m,D} + C_D} \frac{C_A}{K_{m,A} + C_A} \frac{K_{I,H}}{K_{I,H} + C_H} \quad (16)$$

482 Here $K_{I,H}$ is the inhibition coefficient for the inhibiting chemical H . The inhibition term is 1
 483 (not inhibiting) only when $C_H \ll K_{I,H}$. In a system where oxygen and nitrate coexist, which
 484 is common in agriculture lands, aerobic oxidation occurs first before denitrification. The
 485 denitrification rates can be represented by:

$$486 \quad r_{NO_3^-} = \mu_{max} C_{C_5H_7O_2N} \frac{C_D}{K_{m,D} + C_D} \frac{C_{NO_3^-}}{K_{m,A} + C_{NO_3^-}} \frac{K_{I,O_2}}{K_{I,O_2} + C_{O_2}} \quad (17)$$

487 Here $C_{NO_3^-}$ is the concentration of nitrate, K_{I,O_2} is the inhibition coefficient of O_2 , or the O_2
 488 concentration at which it inhibits the reduction of nitrate. This rate law ensures that
 489 denitrification kicks in substantially only when O_2 is depleted to $C_{O_2} \ll K_{I,O_2}$, such that the
 490 term $\frac{K_{I,O_2}}{K_{I,O_2} + C_{O_2}}$ approaches 1.0. If there exists an electron acceptor that is lower in the
 491 redox ladder than nitrate, multiple inhibition terms are needed. environmental conditions
 492 (temperature or soil moisture). For example, for iron oxide, we write the following:

$$493 \quad r_{Fe(OH)_3} = \mu_{max} C_{C_5H_7O_2N} \frac{C_D}{K_{m,D} + C_D} \frac{C_{Fe(OH)_3}}{K_{m,Fe(OH)_3} + C_{Fe(OH)_3}} \frac{K_{I,O_2}}{K_{I,O_2} + C_{O_2}} \frac{K_{I,NO_3^-}}{K_{I,NO_3^-} + C_{NO_3^-}} \quad (18)$$

494 Here K_{I,NO_3^-} is the NO_3^- concentration above which it inhibits iron reduction. The additional
 495 nitrate inhibition term means that iron reduction occurs at significant rates only when both
 496 oxygen and nitrate are low compared to their corresponding inhibition coefficients.

497
 498 **Rates in natural soils.** The dual-Monod and inhibition terms are important under
 499 conditions where electron donors and acceptors are limited. In shallow soil, O_2 is

500 prevalent except under wet conditions with little pore space for air. Anoxic conditions can
 501 also develop in local environments such as dead-end pores where water is saturated for
 502 a long time and not easily flows out. Under conditions in shallow oxic soils where organic
 503 carbon and O₂ are often abundant, the SOM-rate law is for carbon decomposition can be
 504 simplified to the following form assuming microorganism concentrations are relatively
 505 constant:

$$r_{SOM} = \mu_{max} A f r = k A f(T) f(S_w) f(Z_w) \quad (19)(7)$$

507 Where the reaction rate r_{SOM} (r [mol/t] now/s) depends on μ_{max} (rate constant k
 508 [mol/m²/t], s], the lumped surface area A (m²) as an approximation of [m²] is a lumped
 509 parameter that quantitatively represents SOM content and biomass abundance, and $f(T)$
 510 and $f(S_w)$ describe the temperature and soil moisture dependence,
 511 respectively. $f(Z_w)$ can be included to account for the depth distribution of SOM (Seibert
 512 et al., 2009), and Z_w [m] is the water table depth. An example for the depth distribution is
 513 $f(Z_w) \equiv \exp\left(-\frac{Z_w}{b_m}\right)$. For (Weiler and McDonnell, 2006; Ottoy et al., 2016; Bai et al., 2016),
 514 with b_m as the depth coefficient describing the gradient of SOM content over depth. Users
 515 can choose to include either one or all of these dependences in input or database files.

516 The temperature dependence follows a Q₁₀-based form (Friedlingstein et al.,
 517 2006; Hararuk et al., 2015) is commonly used: (Friedlingstein et al., 2006; Hararuk et al.,
 518 2015) as follows:

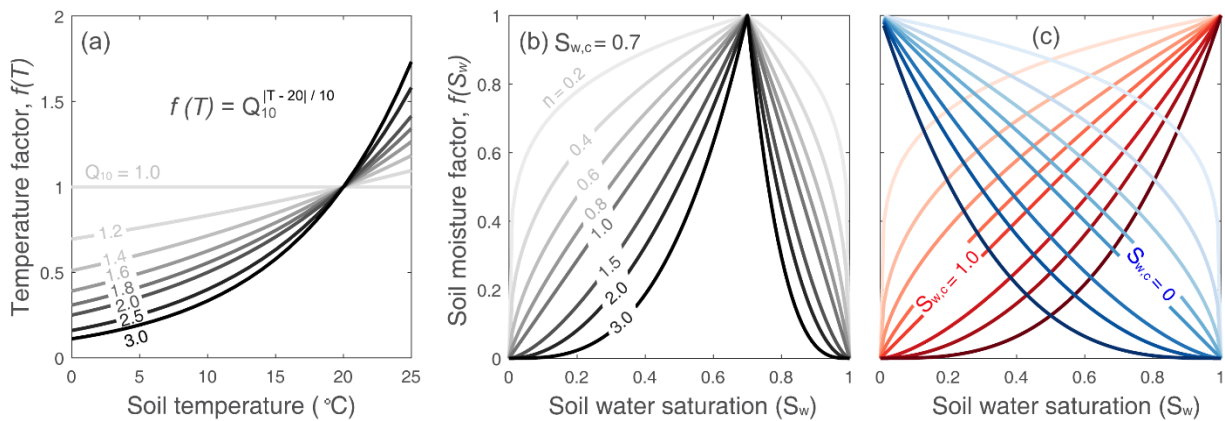
$$f(T) = Q_{10}^{|T-20|/10} \quad (8),$$

519 where Q_{10} is the relative increase in reaction rates when temperature increases by 10 °C
 520 (Davidson and Janssens, 2006). The $f(S_w)$ accounts for the nonlinear (Davidson and
 521 Janssens, 2006). Values of Q_{10} (Figure 4a) can vary from 1.0 to 3.0, depending on
 522 climatic conditions, substrate availability, and ecosystem type (e.g., grassland, forest)
 523 (Davidson et al., 2006; Liu et al., 2017). The mean values are in the range of 1.4 to 2.5
 524 (Zhou et al., 2009; Bracho et al., 2016). The Q_{10} value can be specified in the input file.
 525 The soil moisture dependence of function $f(S_w)$ is coded based on the following form:
 526

527

$$\begin{cases} \left(\frac{S_w}{S_{w,c}}\right)^n, S_w \leq S_{w,c} \\ \left(\frac{1-S_w}{1-S_{w,c}}\right)^n, S_w > S_{w,c} \end{cases} \quad (9)$$

528 Here $S_{w,c}$ [0 to 1] is the critical soil moisture at which rates on soil moisture. A simple form
 529 of $f(S_w) = (S_w)^\epsilon$ where ϵ is the saturation are highest, and n is the exponent (reflecting
 530 the dependence of rates on soil moisture. A typical ϵ value is 2, n value is 2 (Yan et al.,
 531 2018) with a range between 1.5 and 2.5) is 2 and 3.0 (Hamamoto et al., 2010), depending
 532 on soil structure and texture. As shown in Figure 4b, the form indicates an intermediate
 533 critical soil moisture $S_{w,c}$ at which $f(S_w)$ reaches its maximum. When S_w is below this
 534 value, $f(S_w)$ increases with S_w ; when S_w is above this value, $f(S_w)$ decreases with S_w
 535 behavior (Figure 4b) (Yan et al., 2018). Under the extreme conditions of $S_{w,c}$ equals to 0
 536 or 1, $f(S_w)$ monotonically increase or decrease (Figure 4c). The two parameters, $S_{w,c}$ and
 537 n , determines the shape of the curve. They can be specified in input or database files.
 538 One can also choose not to have temperature or soil moisture dependence by choosing
 539 parameters that would lead to the value of exponent being zero.



540

541 **Figure 4.** (a) Function form of soil temperature dependence and (b, c) soil moisture dependence
 542 for reaction rates. The temperature factor $f(T)$ is a function of the Q_{10} (defined by users) and soil
 543 temperature. The soil moisture factor $f(S_w)$ is a function of two user-defined parameters $S_{w,c}$
 544 and n and soil water saturation S_w . The soil moisture function can represent three types of
 545 behaviors: the threshold behavior (b, $0 < S_{w,c} < 1$), increase behavior (red in (c), $S_{w,c} = 1$), and
 546 decrease behavior (blue in (c), $S_{w,c} = 0$). Values of $n = 1$ leads to a linear threshold dependence
 547 of S_w while $n < 1$ and $n > 1$ lead to concave and convex dependences, respectively.

548

549 **Rate dependence on substrates: Monod kinetics and biogeochemical redox**
550 **ladder.** Deeper groundwater aquifers often used. More experience anoxic conditions that
551 lead to processes such as denitrification or methanogenesis. This can also happen in
552 wetlands or wet soils. The rates of microbe-mediated redox reactions depend not only on
553 temperature and soil moisture as discussed above, they also depend on concentrations
554 of electron donors and non-oxygen electron acceptors (e.g., nitrate, iron oxides, sulfate)
555 that are often limited under anoxic conditions (Bao et al., 2014;Li, 2019). The order of the
556 redox reactions often follows the biogeochemical redox ladder, which is based on how
557 much microbe can harvest energy by reducing different types of electron acceptors.
558 Monod reaction rate laws are often used for quantifying rates of these redox conditions.
559 These rate laws are detailed in the section S2 of Supporting Information and also in Li
560 (2019). Users can combine these Monod rate laws and the temperature and soil moisture
561 dependence described above, if needed.

562

563 **3.4 Plant related processes: root uptake of nitrate as an example**

564 Nitrate uptake by plants is intrinsically complex and remains poorly understood
565 (Devienne-Barret et al., 2000;Crawford and Glass, 1998;Hachiya and Sakakibara, 2016).
566 A variety of plant uptake models exists with varying degrees of complexity (Neitsch et al.,
567 2011;Fisher et al., 2010;Cai et al., 2016). These models are mostly based on plant growth
568 module or supply and demand approach that often requires detailed phenological and
569 plant attributes such as growth cycle, root age and biomass, nitrate availability,
570 phosphorous stress, and carbon allocation, in addition to local climate conditions such as
571 temperature and soil moisture (Neitsch et al., 2011;Porporato et al., 2003;Dunbabin et
572 al., 2002;Buysse et al., 1996;Fisher et al., 2010). Without detailed information, we can
573 assume a simple and operational approach (Eqn. 13 and 14). In the Example 2 that we
574 show later, for example, we modeled nitrate uptake with dependence on NO₃⁻
575 concentration, soil temperature and moisture, and rooting density (McMurtrie et al.,
576 2012;Yan et al., 2012;Buljovcic and Engels, 2001).

$$577 \quad r_{\text{uptake}} = k_{\text{uptake}} C_{\text{NO}_3^-} f(T) f(S_w) f_{\text{root}}(d_w) \quad (13)$$

578 $f_{root}(d_w)$ = forms of $f(S_w)$ considering both water limitation under dry conditions and O_2
579 limitation under wet conditions have been proposed (Yan et al., 2018). $\exp((-d_w + \delta) /$
580 $\lambda)$ (14)

581 Where k_{uptake} [L/s] is the nitrate uptake rate, $f_{root}(d_w)$ is the normalized rooting density
582 term in the range of 0 to 1 as a function of water depth to the groundwater (d_w). The
583 rooting term (Eqn. 14) was exponentially fitted ($\delta = 0.013, \lambda = 0.20$) based on field
584 measurements of root distribution along depth (Hasenmueller et al., 2017). It has also
585 been suggested that the decomposition depends strongly on the depth distribution of
586 SOM (Seibert et al., 2009), which is sometime accounted with an additional depth
587 function: is common to observe root density decrease exponentially in forests (López et
588 al., 2001). Other form of user-tailored plant uptake rate law can be added if needed.

589
$$r_{SOM} = \mu_{max} A f(T) f(S_w) f(Z_w) \quad (20)$$

590 where Z_w is the water table depth (m). An example is $f(Z_w) = \exp\left(-\frac{Z_w}{b_{mm}}\right)$ (Weiler and
591 McDonnell, 2006; Ottoy et al., 2016; Bai et al., 2016). Here b_{mm} is the declining coefficient
592 describing the gradient of SOM content over depth.

593

594 4.- Numerical scheme and model verification

595 **Numerical scheme.** The local system of differential equations for water storages [e.g.,
596 Eq. (1), (2), (6), and (7)] on each control volume are combined into a global system of
597 ordinary differential equations (ODEs) and solved in CVODE, a numerical ODE solver in
598 the SUite of Nonlinear and Differential / ALgebraic equation Solvers (SUNDIALS)
599 (Hindmarsh et al., 2005). CVODE is a numerically efficient solver for ODE systems. It
600 uses the backward difference formula (BDF) with adaptive time steps and method order
601 varying between 1 and 5. At each iteration step, the solver evaluates the local error, which
602 is required to satisfy convergence tolerance conditions set by the users. The internal time
603 step is reduced and the method order is adjusted in response to the stiffness of ODEs if
604 the non-convergence occurred. For example, the solver time steps become smaller after
605 heavy precipitation events to address the rapid change of surface and subsurface water
606 storages. The adaptive time stepping and order adjustment scheme make CVODE an

607 ~~accurate and stable solver.~~

608

609 **Model verification.** ~~The BioRT module had been verified against CrunchTope under a~~
610 ~~variety of transport and reaction conditions at a range of reaction complexity levels~~
611 ~~(Supporting Information, Figure S1 – S7). CrunchTope is a widely used subsurface~~
612 ~~reactive transport model (Steefel and Lasaga, 1994; Steefel et al., 2015), and is often used~~
613 ~~as a benchmark to verify other reactive transport models. Verification is~~The system of
614 differential equations for the water storages (e.g., Eqn. 1 and 2, and Eqn. S1 and S2) are
615 assembled into a global system of ordinary differential equations (ODEs) and solved in
616 CVODE (short for C-language Variable-coefficients ODE solver,
617 <https://computing.llnl.gov/projects/sundials/cvode>), a numerical ODE solver in the SUite
618 of Nonlinear and Differential / ALgebraic equation Solvers (SUNDIALS) (Hindmarsh et
619 al., 2005). In BioRT, the transport step is first solved with water by the preconditioned
620 Krylov (iterative) method and the Generalized Minimal Residual Method (Saad and
621 Schultz, 1986). In the following reaction step, all primary species in each finite volume are
622 assembled in a local matrix and then solved iteratively by the Crank-Nicolson and
623 Newton-Raphson method in CVODE (Bao et al., 2017).

624

625 **Model verification.** The BioRT module had been verified against CrunchTope under
626 different transport and reaction conditions (Figures S1 – S7 in SI). CrunchTope is a widely
627 used subsurface reactive transport model (Steefel and Lasaga, 1994; Steefel et al., 2015),
628 and is often used as a benchmark to verify other reactive transport models. Verification
629 was performed under simplified hydrological conditions with 1-D column and constant
630 flow rates such that it focuses on ~~biogeochemical reactive transport processes such as~~
631 advection, diffusion, dispersion, and biogeochemical reactions. Specifically, three cases
632 of soil phosphorus, carbon, and nitrogen were verified for temporal evolution and spatial
633 pattern of relevant solute concentrations ~~(Figure S1 – S7).~~ The soil phosphorus case,
634 which that involves ~~geochemically kinetic and thermodynamic processes (i.e., kinetics-~~
635 ~~controlled~~ apatite dissolution and thermodynamics-controlled phosphorous speciation),
636 was first tested for solution accuracy of the bulk code that was inherited from the original
637 RT-Flux-PIHM. Soil carbon and nitrogen processes that involve ~~microbially-microbe-~~

638 driven processes, such as soil carbon decomposition and mineralization, nitrification and
639 denitrification, were further verified for solution accuracy of the augmented BioRT module.

640

641 **4 Model setup and data needs**

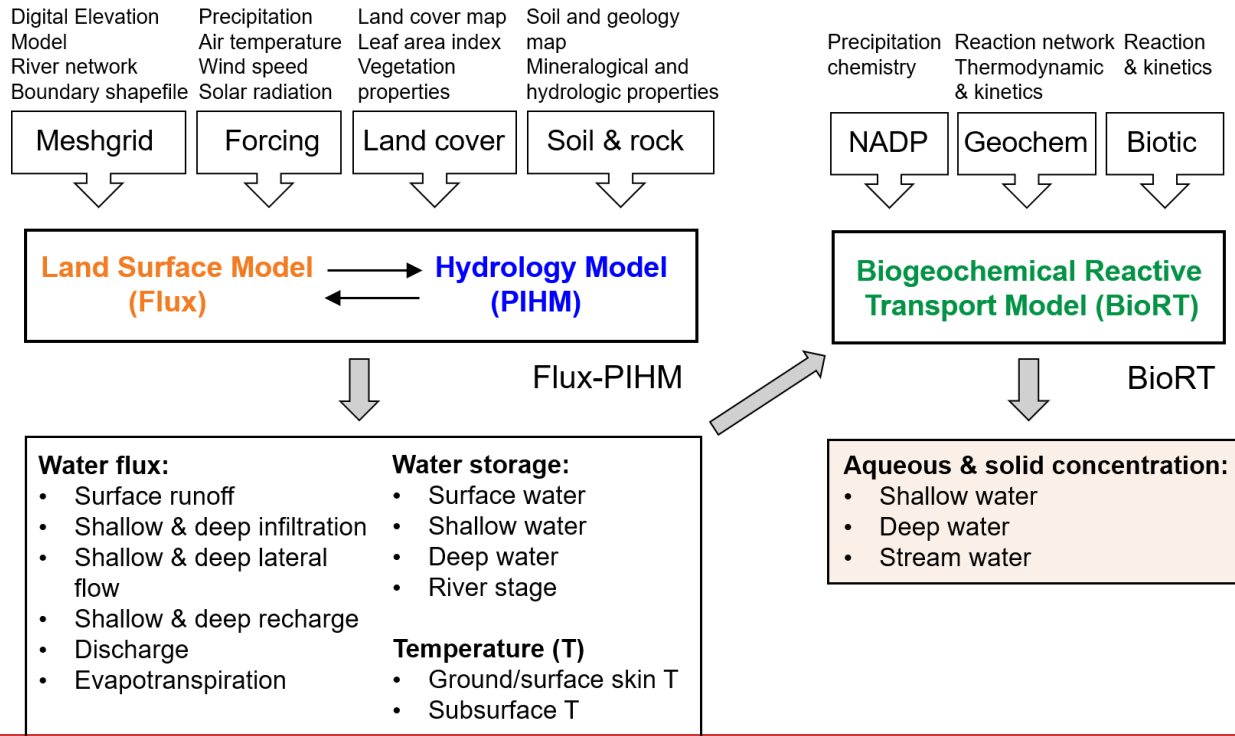
642 **4.15. Model structure, data needs, and input/output**

643 ~~Flux-PIHM sets up the domain based on watershed characteristics including~~
644 ~~topography, hydrography, land cover, and shallow and deep zone properties (Figure 4).~~

645 **4.15.1 Model setup**

646 **Model structure.** The model takes ~~in~~ meteorological forcing time series as input
647 and solves for water storages and soil temperature. ~~BioRT takes, along with other~~
648 hydrologic and land surface states and fluxes (Figure 5). BioRT reads in the model output
649 of water and temperature from Flux-PIHM, and ~~drives~~ solves the ~~simulation for~~
650 biogeochemical reactive transport equations. At the time scale of months to years that
651 are typical for BioRT-Flux-PIHM simulations, ~~the alteration~~ alterations in solid phase
652 properties ~~due to reactions is, including, porosity, permeability, and reactive surface area,~~
653 are considered negligible ~~and does not change such that~~ hydrological parameters ~~remain~~
654 constant with time.

655



656

657 **Figure 4. Data needs.** *The code sets up the model domain based on watershed*
 658 *characteristics including topography, land cover, and shallow and deep zone properties*
 659 *(Figure 5). When the model is used in a spatially distributed form, Model structure, input,*
 660 *and output of BioRT Flux PIHM. The Flux PIHM takes in watershed characteristics including*
 661 *topography (digital elevation model, DEM), land cover, shallow and deep zone properties, and*
 662 *meteorological forcing and then solves for water storage and fluxes, and ground and soil*
 663 *temperature. Water and temperature-related information from Flux-PIHM with additional inputs*
 664 *such as precipitation chemistry and shallow and deep water chemistry and biogeochemical*
 665 *kinetics parameters are then provided for the BioRT module, which eventually outputs aqueous*
 666 *and solid concentration for the shallow and deep zone, and stream water. NADP stands for the*
 667 *National Atmospheric Deposition Program.*

668

669 ~~Most model inputs such as domain can be set up using~~ elevation, land cover, soil
 670 and geology ~~map can be obtained~~ maps supplied by the user or from the data portal of
 671 Geospatial Data Gateway (<https://datagateway.nrcs.usda.gov>). ~~The meteorological~~
 672 ~~forcing data can be downloaded from the North American Land Data Assimilation~~
 673 ~~Systems Phase 2 (NLDAS-2, <https://ldas.gsfc.nasa.gov/nldas/v2/forcing>).~~ The vegetation
 674 ~~forcing, i.e., Leaf Area Index (LAI).~~ ~~The meteorological forcing data can be downloaded~~
 675 ~~from the North American Land Data Assimilation Systems Phase 2 (NLDAS-2,~~

676 ~~<https://ldas.gsfc.nasa.gov/ldas/v2/forcing>~~. The vegetation forcing, i.e., Leaf Area Index
677 (LAI), ~~is~~ can be obtained from ~~the~~ MODIS (Moderate Resolution Imaging
678 Spectroradiometer ~~(,~~ <https://modis.gsfc.nasa.gov/data>). Other vegetation properties
679 associated with land cover (e.g., ~~Other vegetation properties associated with land cover~~
680 ~~(e.g., shading fraction, rooting depth)~~ are can be adopted from, for example, the Noah
681 vegetation parameter table embedded in the Weather Research and Forecasting model
682 (WRF; Skamarock and Klemp (2019)). Local measurements from meteorological stations
683 and field campaigns (e.g., land cover, soil, geology) can also be used in the model.
684 ~~Skamarock and Klemp (2019)). Local measurements from meteorological stations and~~
685 ~~field campaigns (e.g., land cover, soil, geology) can also be used in the model.~~ Another
686 data source ~~for the model input~~ is the HydroTerre (<http://www.hydroterre.psu.edu/>), where
687 users can obtain geospatial data (~~Leonard and Duffy, 2013~~). ~~The form of microbial~~
688 ~~reaction rate laws, when it includes full Monod form, or only with e.g., elevation, land~~
689 ~~cover, geology, soil) (Leonard and Duffy, 2013). Initial water and solid phase chemistry~~
690 ~~can be based on measurements or general knowledge of the simulated sites. The form~~
691 ~~of reaction rate laws, including the Monod form, temperature and soil moisture~~
692 ~~dependence, can be defined in the input files.~~ ~~Additional inputs include initial water and~~
693 ~~solid phase chemistry, description of solutes and biogeochemical reactions, and kinetics~~
694 ~~and~~ and calibrated to reproduce field data. Reaction thermodynamics ~~of reactions, mostly~~
695 equilibrium constants, are from ~~the~~ geochemical database EQ3/6 by default (Wolery,
696 1992). ~~These reaction parameters can be modified when necessary.~~ The model outputs
697 include aqueous and solid concentrations of shallow and deep zone and stream water.
698 ~~The model outputs include aqueous and solid concentrations of shallow and deep~~
699 ~~zone and stream water.~~

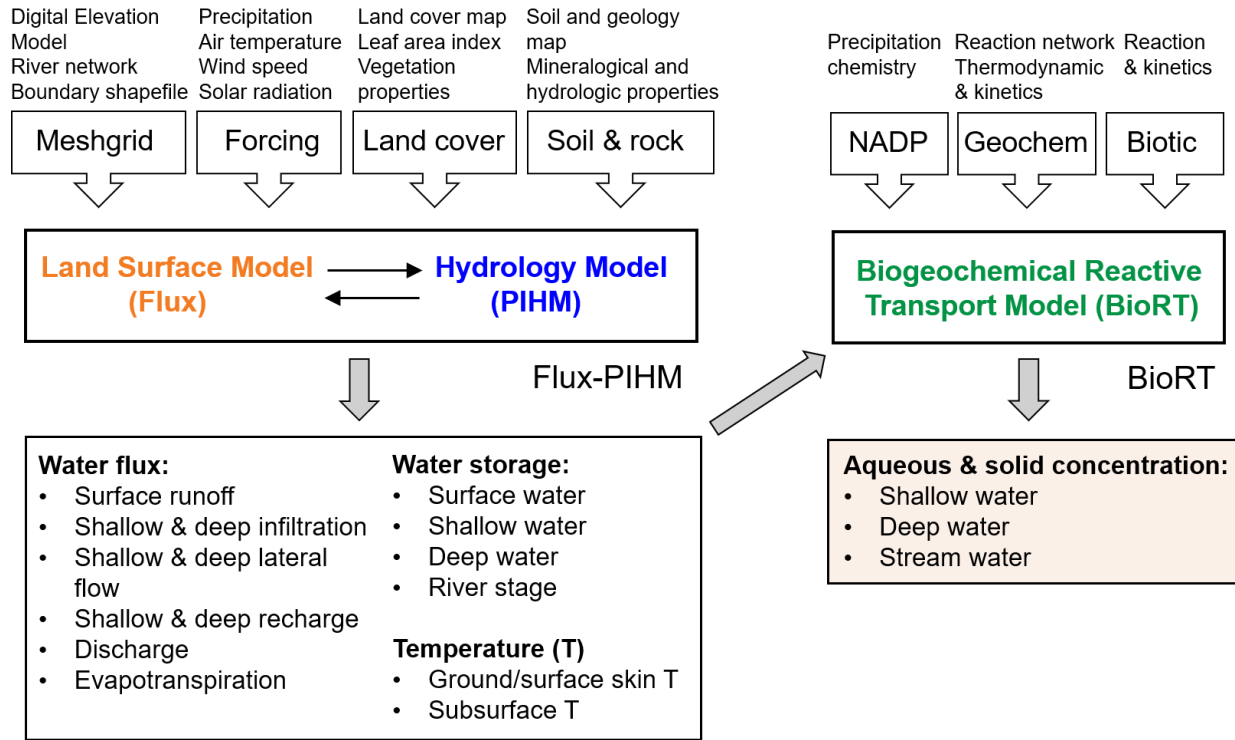


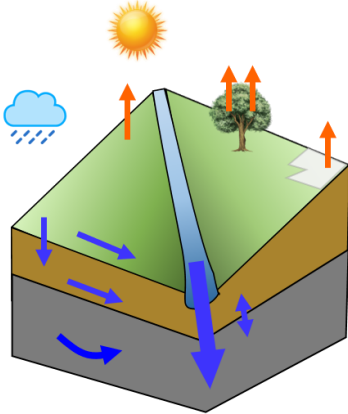
Figure 5. Model structure, input, and output of BioRT-Flux-PIHM. The Flux-PIHM takes in watershed characteristics including topography (digital elevation model, DEM), land cover, shallow and deep zone properties, and meteorological forcing

4.2 Model setup: from simple, spatially implicit to complex, spatially explicit domains

The model domain can be set up using PIHM-GIS (http://www.pihm.psu.edu/pihmgis_home.html), a standalone GIS interface for watershed delineation, domain decomposition, and parameter assignment (Bhatt et al., 2014). The domain can be set up at different spatial resolutions with a different number of grids. A simple domain can be set up with only two land grids representing two sides of a watershed connected by one river cell (Figure 5). This setup uses averaged properties without considering spatial details. This type of model setup requires less spatial data, is computationally inexpensive, and is relatively easy to set up. It can be used to assess the average dynamics of the water and solute dynamics and focus on the interactions among processes without concerning spatial details. It can also be used as a relatively easy starter for educational purposes before students jump into complex domains. Alternatively, a complex domain can be set up using many grids with explicit

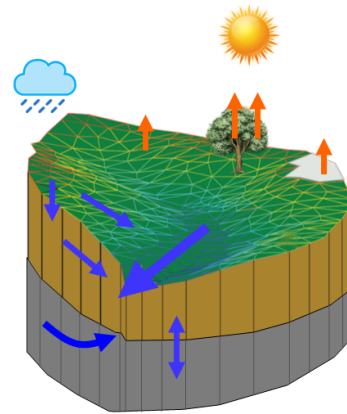
718 representation of spatial details. It requires much more data and is computationally
719 expensive but can be used to identify “hot spots” of biogeochemical reactions.

Simple configuration: spatially implicit mesh (2 land + 1 river cells)



Homogenized properties

Complex configuration: spatially explicit mesh (multiple land and river cells)



Heterogenized properties

Same model processes could be realized in both configurations:

- Land-surface process
- Hydrological process
- Biogeochemical process

720
721 **Figure 5.** Two extreme model domain setups: a simple domain with two land cells representing
722 two hillslopes connected by one river cell, versus a complex domain with hundreds of land cells.
723 An intermediate number of grids can also set up the domain, depending on watershed
724 heterogeneity, data availability, and desired spatial resolution.

725
726 5time series and solves for water storage, and ground and soil temperature. BioRT takes in water-
727 and temperature-related information from Flux-PIHM with additional inputs such as precipitation
728 chemistry and shallow and deep water chemistry and biogeochemical kinetics parameters, and
729 solve for aqueous and solid concentrations in the shallow and deep zone, and stream water.
730 NADP stands for the National Atmospheric Deposition Program. This paper focuses on the BioRT
731 component. The land-surface, hydrological processes, and abiotic reactive transport processes
732 have been described in previous papers (Bao et al., 2017;Shi et al., 2013). Discussions on how
733 air temperature and ET influence stream chemistry can be found in Li (2019).

734
735 **Domain set up: from simple, spatially lumped to complex, spatially distributed**
736 **domains.** The domain can be set up at different spatial resolutions with different numbers
737 of grids. A simple domain can be set up with only two land grids representing two sides
738 of a watershed connected by one river cell. This setup uses averaged properties without
739 needs for larger spatial data. Alternatively, a complex domain can be set up using many
740 grids with explicit representation of spatial details. The model domain can be set up using

741 PIHM-GIS (http://www.pihm.psu.edu/pihmgis_home.html), a standalone GIS interface for
742 watershed delineation, domain decomposition, and parameter assignment (Bhatt et al.,
743 2014). It requires much more data and can be computationally expensive but can be used
744 to identify “hot spots” of biogeochemical reactions within a watershed. The same model
745 processes (e.g., hydrology, reaction network) can be setup in both spatial configurations.
746 Auto-calibration is not built into the model, but a global calibration coefficient approach is
747 used to reduce parameter dimension and facilitate manual calibration. A typical model
748 application requires 20 to 30 hydrological parameters to be calibrated. These parameters
749 include land surface parameters (e.g., canopy resistance, surface albedo), soil and
750 geology parameters (e.g., hydraulic conductivity, porosity, Van Genuchten, macropore
751 properties) (Shi et al., 2013). Reaction-related parameters (e.g., reaction rate constant,
752 mineral surface area, Q_{10} , $S_{w,c}$, and n) are additionally needed for calibration, the number
753 of which depends on the numbers of reactions involved in a particular system.

754

755 **6. Model applications**

756 The original RT-Flux-PIHM has been applied to understand ~~the~~ processes related
757 to ~~the~~ geogenic solutes of Cl and Mg at the Shale Hills watershed and for ~~geogenic~~-Na ~~at~~
758 ~~the~~in a watershed on Volcán Chimborazo ~~watershed~~in the Ecuadorian Andes (Table 1).
759 The new BioRT-Flux-PIHM has been demonstrated for understanding the dynamics of
760 DOC, and nitrate, ~~and Na~~ at Shale Hills and Coal Creek. This section ~~presents some new~~
761 ~~model features using two~~ will present one hydrology and two biogeochemical ~~examples:~~
762 ~~one with a simple, spatially implicit domain, and another with a complex, spatially explicit~~
763 ~~domain.~~ in the Susquehanna Shale Hills Critical Zone Observatory (SSHCZO), a
764 small headwater watershed in central Pennsylvania, USA. The mean annual precipitation
765 is approximately 1,070 mm and the mean annual temperature is 10 °C (Brantley et al.,
766 2018). Soil carbon storage and respiration and nitrogen budget and fluxes have been
767 studied in detail (Andrews et al., 2011; Hasenmueller et al., 2015; Shi et al., 2018; Hodges
768 et al., 2019; Weitzman and Kaye, 2018). Modeling work has been conducted to
769 understand hydrological dynamics (Shi et al., 2013; Xiao et al., 2019), transport of the non-
770 reactive tracer Cl, and the weathering-derived solute Mg (Bao et al., 2017; Li et al., 2017a).

771 **Table 1. Existing Model applications with different biogeochemical reactions of BioRT-Flux-**
 772 **PIHM**

Watershed (location)	Size (km ²)	Model domain	Modeled solutes	Reaction network (Kinetic Reactions (rate laws: 1, TST; 2, Monod based; 3, plant uptake-rate))	Reference
Shale Hills (PA, USA)	0.08	Complex (535 grids) Spatially distributed	Cl, Mg	<ul style="list-style-type: none"> Chlorite dissolution¹ Illite dissolution¹ Carbonate dissolution & precipitation¹ Cation exchange 	Bao et al., 2017; Li et al., 2017
		Complex (535 grids) Spatially distributed	DOC	<ul style="list-style-type: none"> SOC decomposition² DOC sorption 	Wen et al., 2020
		Simple (2 grids) Spatially lumped	NO ₃ ⁻	<ul style="list-style-type: none"> Soil N leaching² Denitrification² Plant nitrate-uptake³ 	This work
Coal Creek (CO, USA)	53	Simple (2 grids) Spatially lumped	DOC, Na	<ul style="list-style-type: none"> SOC decomposition² DOC sorption Albite dissolution¹ 	Zhi et al., 2019
Volcán Chimborazo (Ecuador)		Complex (160 grids) Spatially distributed	Cl, Na, Ca, Mg, SiO ₂	<ul style="list-style-type: none"> Albite dissolution¹ Diopside dissolution¹ 	Leila et al., 2020 (under review) Saberi et al. (under review)

773 Note: Transition State Theory (TST) is a classic kinetic rate law for mineral dissolution and
 774 precipitation (~~Brantley et al., 2008~~); Monod based (~~Brantley et al., 2008~~) (Eqn. S15); Monod rate
 775 law with environmental dependency (i.e., soil temperature and soil moisture) is widely used for
 776 ~~microbial/microbially~~ driven reactions; ~~plant nitrate uptake depends on nitrate availability,~~
 777 ~~environmental dependency, and rooting depth.~~ Monod-based and plant nitrate uptake rate law
 778 are detailed in the following section of 5.1.16.2. SOC stands for soil organic carbon.

779

780 Here we present two examples of different processes in the Susquehanna Shale
781 Hills Critical Zone Observatory (SSHCZO), a small headwater watershed (0.08 km²) in
782 central Pennsylvania, USA. The mean annual precipitation is approximately 1,070 mm
783 and the mean annual temperature is 10 °C. Extensive field measurements have been
784 conducted to characterize the topography, vegetation, and bedrock and soil properties
785 (Brantley et al., 2018). Soil carbon storage and respiration and nitrogen budget and fluxes
786 have been detailed studied (Andrews et al., 2011; Hasenmueller et al., 2015; Shi et al.,
787 2018; Hodges et al., 2019; Weitzman and Kaye, 2018). Modeling work has also been
788 conducted to understand hydrological dynamics (Shi et al., 2013), transport of a non-
789 reactive tracer Cl and the soil and rock weathering Cl and Mg (Bao et al., 2017; Li et al.,
790 2017a).

791

792 **5.1 Hydrology Example: Shallow and deep water interactions**

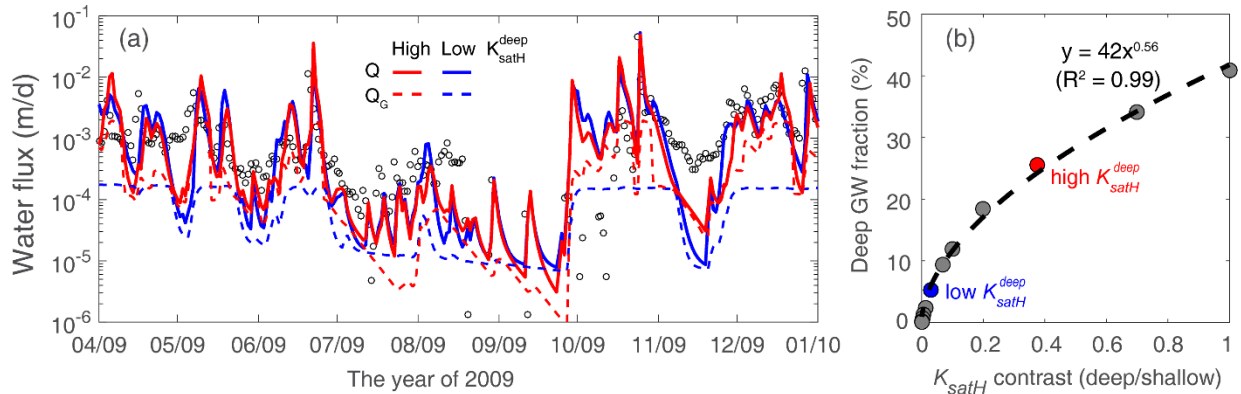
793 **6.1 Example 1: Shallow and deep water interactions**

794 The model was set up using the spatially lumped mode with two land grids and
795 one river grid, represented characterized by the averaged average land cover, soil and
796 rock properties based on previous work (Shi et al., 2013; Kuntz et al., 2011). Specifically,
797 the model (Shi et al., 2013; Kuntz et al., 2011). The model assumed a Weikert soil, the
798 dominant soil type at Shale Hills (Shi et al., 2013). (Shi et al., 2013). The porosity of the
799 deep zone was set to 1/10a tenth of the shallow soil porosity based on measurements of
800 the deep subsurface (Brantley et al., 2018; Kuntz et al., 2011). Stream discharge and ET
801 observations were used to calibrate hydrological parameters (Figure S9). Groundwater
802 (Q_G) from the deep layer was constrained by previous work (Li et al., 2017a) and the
803 nitrate concentration discharge (C-Q) observations. Important land surface and
804 hydrological parameters are summarized in Table S7.

805 **Water budget.** The model reproduced the seasonal dynamics of discharge and ET
806 (Figure S9), with daily Nash-Sutcliffe efficiency (NSE) of 0.56 and 0.66, respectively.
807 Precipitation occurs throughout the year while the discharge was responsive to a few big
808 storm events in spring and fall. The ET peaked during the summer due to higher solar

809 radiation and higher temperature while declined in the fall and winter. The runoff ratio was
810 0.46, suggesting 46% of precipitation was discharged through the stream while the
811 remaining 54% contributed to ET. A breakdown analysis suggests at the annual scale,
812 the shallow lateral flow (Q_L , 87% of Q) dominated discharge, followed by the deeper
813 groundwater flow (Q_G , 9.3%), and the surface runoff (Q_S , 4.2%). The Q_G was essential in
814 maintaining discharge during dry time, especially in the summer.

815 Controls of deep water aquifer (Brantley et al., 2018; Kuntz et al., 2011). In a
816 headwater watershed catchment like Shale Hills where the deep groundwater is most
817 likely sourced from recharge, the deep groundwater contribution to the stream was can be
818 primarily controlled by the hydraulic conductivity (K_{satH}) contrast between the deep and
819 shallow zone zones (i.e., $K_{satH}^{deep} / K_{satH}^{dp} / K_{satH}^{shallow}$). Because K_{satH}^{sl} . This is because the
820 K_{satH} contrast determined determines the partitioning of infiltrating water between the
821 shallow lateral flow and the downward recharge to the deep zone and then deep
822 groundwater flow. Two cases of high (red) and low (blue) $K_{satH}^{deep} K_{satH}^{dp}$ were set up to
823 showcase the control of K_{satH} contrast control on deep groundwater (Figure 6a). By
824 changing the deep zone $K_{satH}^{deep} K_{satH}^{dp}$ from 2.6 to 0.22 (m/d), about 38% and 3.1% of the
825 shallow zone $K_{satH}^{shallow}$, the annual deep groundwater (Q_G) contribution to discharge (Q)
826 decreased from 26% to 5.2%, respectively. It is also noticeable although the total
827 discharge is negligible. This indicates that there was minimal change between discharge
828 (i.e., solid lines in Figure 6a) as the deep zone K_{satH}^{deep} does not affect shallow water
829 partitioning for infiltrating water and discharge. This new hydrology feature enables the
830 exploration of the interaction between deep groundwater and surface water. These
831 features can be used to understand watersheds of different subsurface structures and
832 with deep water the changing K_{satH}^{dp} mostly from changes the portioning between the
833 shallow soil lateral flow and recharge. In addition, they can be used to explore large
834 watersheds of higher stream order with a large proportion of deep water coming from
835 nearby regional aquifers., whereas total infiltration and discharge remain very similar.



836

837 **Figure 6.** (a) Hydraulic conductivity (K_{satH}) contrast control on deep groundwater (Q_G). The cases
 838 of high ($K_{satH}^{dp} = 2.6 \text{ m/d}$, red) and low conductivity ($K_{satH}^{dp} = 0.22 \text{ m/d}$, blue) K_{satH}^{deep} led to 26%
 839 and 5.2% of annual Q_G contribution to discharge (Q), respectively. (b) Deep groundwater fraction
 840 as a function of K_{satH} contrast between the deep and shallow zone. The K_{satH} contrast was
 841 limited to 1 in the figure as most watersheds exhibit a smaller K_{satH} in the deep zone than in the
 842 shallow zone. The two red and blue dots correspond to the two cases in left panel.

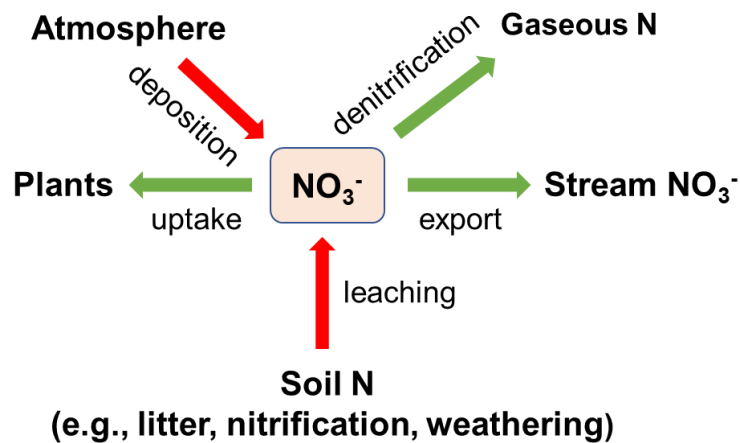
843

844 ~~A series of similar~~ Several additional cases were further tested to ~~generate~~ examine
 845 the relationship between deep groundwater fraction (%) of discharge and K_{satH} contrast
 846 (Figure 6b). ~~Results show~~ shows that the deep groundwater fraction exponentially
 847 increased rapidly increases with the increasing K_{satH} ~~contrast~~ ratio of $K_{satH}^{dp} / K_{satH}^{sl}$,
 848 reaching a limit at when K_{satH} contrast is sufficiently high. ~~The results also suggest that~~
 849 ~~the maximum~~ The deep groundwater contribution to the stream was limited to reaches ~
 850 40% ~~as most watersheds exhibit smaller K_{satH}^{deep} than $K_{satH}^{shallow}$~~ . The fitting function (dashed
 851 line) ~~could be a useful predictor to quantify deep~~ when the K_{satH}^{dp} and K_{satH}^{sl} are equal. In
 852 natural systems, we do see places, for example, karst formations, where groundwater
 853 contribution at headwater watersheds given measured deep and shallow
 854 hydraulic contributes to more than 40% (Hartmann et al., 2014; Husic, 2018). These places
 855 may have higher deeper conductivity than shallow soils due to the development of highly
 856 conductive conduits.

857

858 **56.2 Reactive Transport Example 1: Understanding nitrate 2: Nitrate dynamics**
 859 **using** in a spatially implicit domain

860 This example focuses on nitrate, ~~which is the~~ (NO_3^-), a dominant dissolved N form
 861 in water ~~and has relatively with~~ abundant measurements ~~from 2008 to 2010~~
 862 (<https://criticalzone.org/shale-hills/data/datasets/>) ~~(Weitzman and Kaye, 2018).~~ ~~Based on~~
 863 ~~their~~ (Weitzman and Kaye, 2018). The N processes at Shale Hills include atmospheric N
 864 deposition, soil N leaching, stream export, denitrification, and plant uptake (Figure 7).
 865 Based on field measurements, the atmospheric deposition ~~was at the site is~~ the dominant
 866 N input and N export via discharge ~~was is~~ only a small fraction (2.5%) of atmospheric N
 867 input. ~~Most, indicating most~~ deposited N ~~was either is~~ tightly cycled by plants or lost to
 868 the atmosphere via denitrification ~~or uptaken by trees.~~ ~~The model at Shale Hills watershed~~
 869 ~~included atmospheric N deposition, soil N leaching, stream export, denitrification, and~~
 870 ~~plant uptake (Figure 7).~~



871 **Figure 7.** Modeled nitrogen processes ~~at Shale Hills in Example 2.~~ Atmospheric N deposition
 872 ~~was is~~ the major N ~~sources (top red arrows); input;~~ denitrification and plant uptake ~~were are~~ the
 873 major N loss and sink ~~(green arrows).~~ Export ~~from via~~ discharge ~~removes nitrate but it was a~~
 874 ~~relatively only occupies a small one fraction.~~

875
 876
 877 The soil N leaching process was represented using a lumped reaction that
 878 generates NO_3^- . Conceptually this could represent the total rates of reactions including
 879 the decomposition of soil organic matter (SOM), nitrification, and rock weathering that
 880 generates NO_3^- . Its rate was assumed to depend on soil temperature and moisture and
 881 follows the equation $r_{leach} = kAf(T)f(S_w)$, where r_{leach} [mol/s] is the leaching rate, $k =$
 882 $10^{-9.7}$ [mol/m²/s] is the leaching rate constant (Regnier and Steefel, 1999), and A [m²] is
 883 the surface area that represents the contact area between substrates and N transforming

884 microbe, and $f(T)$ and $f(S_w)$ are soil temperature (Eqn. 8) and soil moisture (Eqn. 9)
 885 functions, respectively. The surface area was calculated based on SOM volume fraction
 886 $[m^3/m^3]$, specific surface area (SSA, $[m^2/g]$), substrate density $[g/cm^3]$, and element
 887 volume $[m^3]$. Denitrification converts NO_3^- to N_2 gas under anaerobic conditions. Here this
 888 process was modeled by the Monod rate law with DOC as the electron donor (Di Capua
 889 et al., 2019), NO_3^- as the electron acceptor, and with an inhibition term $f(O_2)$ (Eqn. S13).
 890 The reaction rate: $r_{denitrification} = kA \frac{C_{DOC}}{K_{m,DOC} + C_{DOC}} \frac{C_{NO_3^-}}{K_{m,NO_3^-} + C_{NO_3^-}} f(O_2) f(T) f(S_w)$, where $k =$
 891 10^{-10} $[mol/m^2/s]$ is the denitrification rate constant (Regnier and Steefel, 1999), half-
 892 saturation constants $K_{m,DOC} = 15$ $[uM]$ and $K_{m,NO_3^-} = 45$ $[uM]$ (Regnier and Steefel,
 893 1999;Billen, 1977). For soil N leaching and denitrification, the SSA were respectively
 894 tuned as 1.6×10^{-6} and 7.5×10^{-5} $[m^2/g]$ to reproduce observed stream nitrate dynamics.
 895 The calibrated values were orders of magnitude lower than the lab measured SSA of
 896 natural materials (e.g., SOM, $0.6 \sim 2$ m^2/g) (Rutherford et al., 1992;Chiou et al., 1990).
 897 Such discrepancies between calibrated effective reactive surface area (i.e., The soil N
 898 leaching process was a lumped reaction that generates NO_3^- source, including the
 899 decomposition of soil organic matter (SOM), nitrification, and rock weathering. Its rate
 900 was assumed to depend on soil temperature and moisture:

$$901 \quad r_{leach} = kA f(T) f(S_w) \quad (21)$$

902 Here r_{leach} is the leaching rate (mol/s), k is the rate constant (mol/m²/s), and the surface
 903 area A (m²) is a lumped parameter representing the effective contact area between
 904 substrates and N transforming microbe. It was calculated based on SOM volume fraction
 905 (m³/m³), specific surface area (SSA, m²/g), substrate density (g/cm³), and element
 906 volume (m³).

907 ~~———— The denitrification process converts NO_3^- to N_2 gas under anaerobic conditions.~~
 908 ~~This process can be modeled by the Monod rate law with nitrate as the electron acceptor~~
 909 ~~substrate ($K_{m,NO_3^-} = 45$ uM (Regnier and Steefel, 1999;Billen, 1977)) and with inhibition~~
 910 ~~from O_2 (Eq. (22)). Under conditions where O_2 concentration is not explicitly modeled (this~~
 911 ~~work), the O_2 inhibitory term can be replaced by a function of soil moisture (Eq. (24)). This~~
 912 ~~is based on field evidence that denitrification typically occurs when soil moisture is greater~~

913 than 0.6 and increases with increasing soil moisture (Brady et al., 2008). Equation (24)
 914 says that under relatively drier conditions ($S_w < 0.6$), there is sufficient O_2 that
 915 denitrification does not occur; under wet conditions ($S_w \geq 0.6$), the O_2 becomes limiting
 916 such that denitrification can occur.

$$917 \quad r_{denitrification} = kA \left(\frac{C_{NO_3^-}}{K_{m,NO_3^-} + C_{NO_3^-}} \right) f(O_2) f(T) f(S_w) \quad (22)$$

$$918 \quad f(O_2) = \frac{K_{T,O_2}}{K_{T,O_2} + C_{O_2}} \quad (23), \text{ when } O_2 \text{ is explicitly modelled}$$

$$919 \quad f(O_2) = \frac{\theta (S_w < 0.6)}{(S_w - 0.6) * 2.5 (S_w \geq 0.6)} \quad (24), \text{ when } O_2 \text{ is not explicitly modelled}$$

920
 921 ——— Nitrate uptake by plants is intrinsically complex and not yet completely understood
 922 (Devienne-Barret et al., 2000; Crawford and Glass, 1998; Hachiya and Sakakibara, 2016).
 923 A variety of plant uptake models exists in literature with varying levels of complexity
 924 (Neitsch et al., 2011; Fisher et al., 2010; Cai et al., 2016). These models are mostly based
 925 on plant growth module or supply and demand approach that often requires detailed
 926 phenological and plant attributes such as growth cycle, root age and biomass, nitrate
 927 availability, phosphorous stress, and carbon allocation, in addition to local climate
 928 conditions such as temperature and soil moisture (Neitsch et al., 2011; Porporato et al.,
 929 2003; Dunbabin et al., 2002; Buysse et al., 1996; Fisher et al., 2010). Without all the
 930 detailed information, here we assumed a simple and operational approach to model
 931 nitrate uptake with dependence on NO_3^- concentration, soil temperature and moisture,
 932 and rooting density (Eq. (25), (26)). More detailed, user-tailored plant uptake rate law can
 933 be added if needed.

934 r_{uptake} = solid-water contact area) and lab measured absolute surface area are
 935 consistent with other observations in literature (Li et al., 2014; Heidari et al., 2017). The
 936 uptake rate constant was calibrated by constraining the partitioning of N transformation
 937 flux between denitrification and plant uptake by the ratio of 1:5, a value estimated from
 938 field measurements of gaseous N outputs (3.53 kg-N/ha/yr) and plant N uptake (18.3 kg-
 939 N/ha/yr) (Weitzman and Kaye, 2018). The uptake rate constant in the deep zone (> 2 m

940 in depth) was considered negligible (Weitzman and Kaye, 2018;Hasenmueller et al.,
941 2017). Groundwater nitrate was initialized as 0.43 mg/L, the average of measured
942 groundwater concentration during 2009 - 2010.

$$943$$
$$944 \quad k_{uptake} C_{NO_3^-} f(T) f(S_w) f_{root}(d_w) \quad (25)$$

$$945 \quad f_{root}(d_w) = \exp((-d_w + r)/s) \quad (26)$$

946 ~~Where k_{uptake} is the nitrate uptake rate (L/s), $f_{root}(d_w)$ is a normalized rooting density~~
947 ~~term in the range of 0 to 1 as a function of water depth to the groundwater (d_w). The~~
948 ~~rooting term (Eq. (26)) was exponentially fitted ($r = 0.0132, s = 0.202$) based on field~~
949 ~~measurements of root distribution along depth (Figure S8) (Hasenmueller et al., 2017).~~
950 ~~The exponentially declining root function is generally to be the case in forested~~
951 ~~watersheds but can be tailored to agricultural watersheds when field data are available.~~

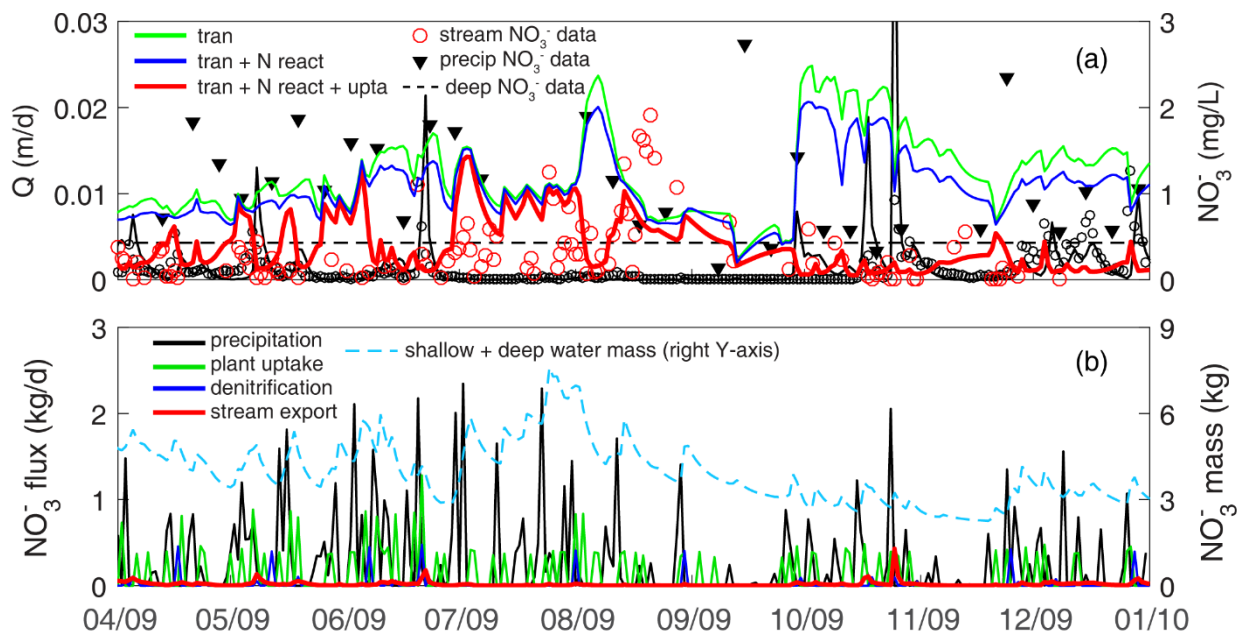
952 ~~For microbial soil N leaching and denitrification, reaction rate constant k was~~
953 ~~specified (Regnier and Steefel, 1999) and the lumped surface area A (m^2 , = specific~~
954 ~~surface area $m^2/g \times g$ of mass) was turned to reproduce stream nitrate dynamics and its~~
955 ~~C-Q pattern (Table S8). The calibrated effective specific surface area (SSA) were orders~~
956 ~~of magnitude lower than the lab measured SSA of natural materials (e.g., SOM, 0.6–2~~
957 ~~m^2/g) (Rutherford et al., 1992; Chiou et al., 1990). ~~Such discrepancies between calibrated~~~~
958 ~~effective reactive surface area (i.e., solid-water contact area) and lab measured absolute~~
959 ~~surface area are consistent with other observations (Li et al., 2014; Heidari et al., 2017).~~
960 ~~The nitrate uptake rate constant k_{uptake} was calibrated to constrain the partitioning of N~~
961 ~~transformation flux between denitrification and plant uptake by the ratio of 1:5, a value~~
962 ~~estimated from field measurements of gaseous N outputs (3.53 kg-N/ha/yr) and plant N~~
963 ~~uptake (18.3 kg-N/ha/yr) (Weitzman and Kaye, 2018). We assumed that the nitrate uptake~~
964 ~~rate k_{uptake} of the deep zone (> 2 m in depth) was 1/1000 of that in the shallow zone,~~
965 ~~based on the observations that the rooting density exponentially decrease with depth~~
966 ~~(Weitzman and Kaye, 2018;Hasenmueller et al., 2017). Groundwater nitrate was~~
967 ~~initialized as 0.43 mg/L, the average of measured groundwater concentration during~~
968 ~~2009-2010.~~

969 **Temporal nitrate dynamics.** Three cases were set up to understand and quantify the
970 effects of different processes in determining ~~the~~ nitrate dynamics (Figure ~~88a~~). The
971 *transport-only* case (~~greendashed~~ line, *tran*) ~~only has N~~ simulates nitrate input from
972 precipitation (at 1.4 ± 0.96 mg/L, based on the 2009 data of NADP PA42 site) and N
973 transport but without any reactions. It overestimated stream nitrate data (0.33 ± 0.39
974 mg/L) throughout the year. The *transport + N reactions* case (~~bluegray~~ line, *tran + N react*)
975 has ~~the~~ denitrification and soil N leaching processes but not plant uptake. ~~It~~ These two
976 reactions lowered the nitrate concentration, ~~suggesting their relative minor role slightly,~~
977 as these two processes compensate each other in ~~controlling N~~ adding and removing
978 nitrate from water. The *transport + N reactions + uptake* case (~~redthick black~~ line, *tran +*
979 *N react + upta*) have all processes. It significantly lowered the nitrate concentration,
980 especially in April-May and October-December. ~~There were some overestimated short~~
981 nitrate Nitrate peaks from May to July, exhibiting comparable levels of high precipitation
982 nitrate concentration (Figure ~~8a8b~~). It is noticeable that the three cases (~~i.e., transport-~~
983 ~~only, transport + N reactions, transport + N reactions + uptake~~) almost overlapped (~~i.e.,~~
984 ~~minimal difference~~) at these overestimated short nitrate peaks, suggesting ~~the~~ nitrate-rich
985 precipitation was may not be routed into the subsurface where denitrification and plant
986 uptake could occur ~~and lower the nitrate concentration. In short, hydrology controlled~~
987 ~~stream nitrate dynamics by partitioning the nitrate-rich precipitation into surface runoff,~~
988 ~~shallow lateral flow, and deep groundwater. Nitrate reactions primarily controlled stream~~
989 ~~concentration via the subsurface flow flowpath where the nitrate-rich precipitation~~
990 ~~undergone significant nitrate loss and sink, as denitrification and plant uptake only~~
991 ~~occurred to remove nitrate in the subsurface but not in surface water.~~

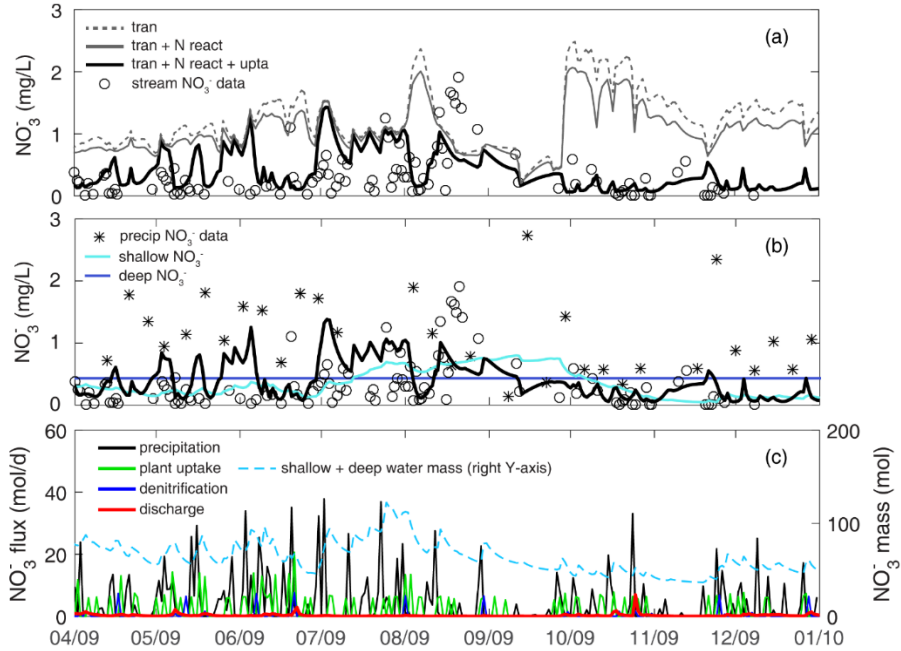
992 Comparing the three outfluxes (Figure ~~8b~~), ~~nitrate export via discharge (red) was~~
993 ~~negligible compared to denitrification (blue) and plant uptake (green). At the annual scale,~~
994 ~~stream nitrate export only accounted for 9.5% outfluxes, whereas denitrification and plant~~
995 ~~uptake took up 15% and 75% of precipitated NO_3^- , respectively. At Shale Hills, rock N~~
996 ~~leaching (weathering) is calculated up to 10% of N precipitation.~~

997 Although precipitation ~~source occurred primarily~~ from April to August (accounted
998 for 70% of the total simulation period), larger storm events in October contributed more
999 to the export. Deeper groundwater had higher nitrate concentration than shallow water,

1000 because most plant uptake occurred in the shallow zone. The nitrate fluxes into the
 1001 deeper zone however only contributed 26% of stream nitrate export at the annual scale,
 1002 due to the relatively small groundwater contribution (9.5%) to the stream. Denitrification
 1003 and plant uptake largely occurred during the wet ~~period, which coincided with the growing~~
 1004 ~~season. Denitrification peaks often showed up after major storm events. spring period,~~
 1005 ~~which is part of the leaf-on season. Denitrification peaks often appeared after major storm~~
 1006 ~~events. Comparing the three outfluxes (Figure 8c), nitrate export via discharge (red) was~~
 1007 ~~negligible compared to denitrification (blue) and plant uptake (green). At the annual scale,~~
 1008 ~~stream export only accounted for 9.5% outfluxes, whereas denitrification and plant uptake~~
 1009 ~~took up 15% and 75% of deposited NO_3^- , respectively. In other words, as Nitrate enters~~
 1010 ~~this system via precipitation, plant uptake can play a significant role in reducing nitrate~~
 1011 ~~level, indicating precipitated nitrate is tightly cycled in the system.~~



1012



1013

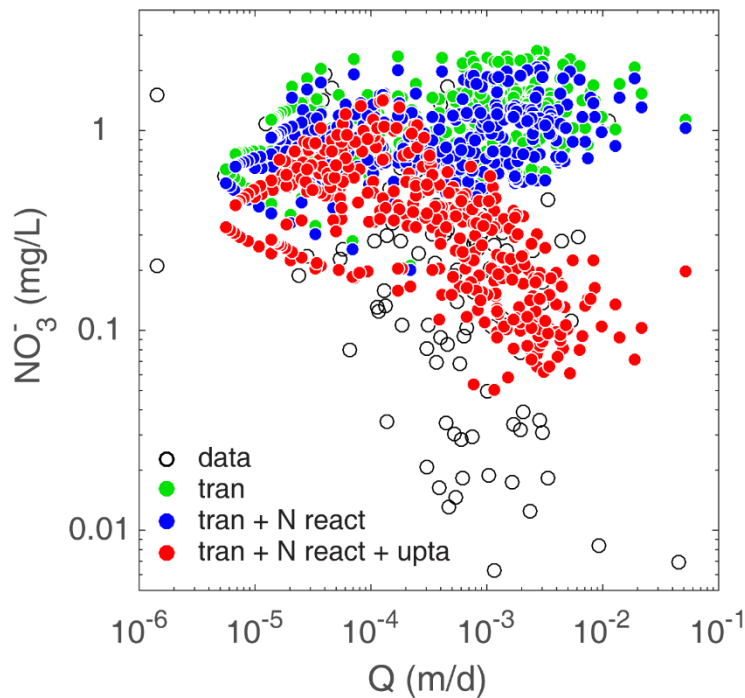
1014 **Figure 8.** Stream nitrate dynamics and fluxes at Shale Hills in Example 2. (a) stream nitrate
 1015 dynamics in three simulation conditions with different processes: transport-only (green dashed
 1016 line, tran), transport + N reaction (blue gray line, tran + N react), transport + N reaction + plant
 1017 uptake (red thick black line, tran + N react + upta), where N reactions include both nitrate leaching
 1018 and denitrifications—denitrification (see Figure 8). (a) stream nitrate dynamics; (b) nitrate
 1019 concentration in precipitation, shallow and deep water; (c) nitrate fluxes and budget. Note the
 1020 nitrate leaching was ignored in (b) due to its minimal flux as precipitation N deposition was as the
 1021 dominant input source (Weitzman and Kaye, 2018). (Weitzman and Kaye, 2018).

1022

1023 **C-Q patterns.** ~~C-Q plots from the three cases showed distinct patterns (Figure 9). Specifically, the transport-only (green) and transport + N reactions (blue) cases led to chemostatic or slightly flushing patterns while the transport + N reactions + plant uptake (red) case showed a dilution pattern similar to field observation. The transport-only case showed a slightly flushing pattern because the shallow water had slightly higher nitrate concentration (directly from precipitation without reactions) than deep groundwater. This results in low stream concentrations from deep groundwater at low flow conditions and high stream concentrations from shallow water with higher nitrate at high flow conditions. With limited denitrification capacity (Figure 8a), the transport + N reactions case was similar to the transport-only case. In comparison, the plant uptake reduced nitrate~~

1032

1033 concentration in the shallow zone, to an extent lower than the concentration in the deeper
1034 zone, altering the C-Q pattern from primarily chemostatic to dilution (Figure 9).



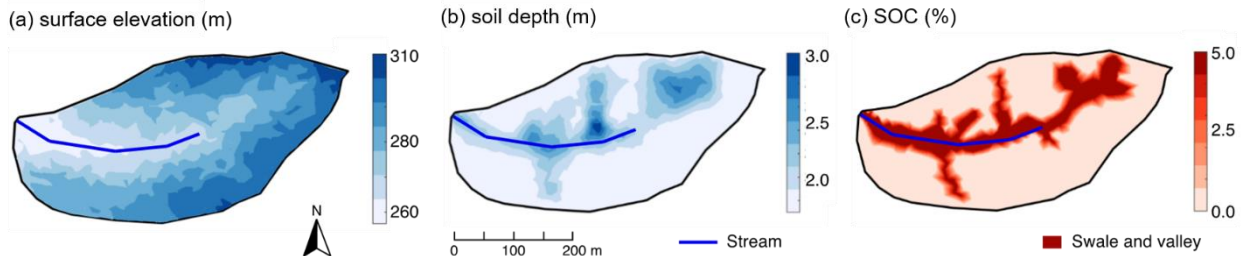
1035
1036 **Figure 9.** Concentration-discharge (C-Q) relationships under three scenarios that involve different
1037 processes: transport-only (green, *tran*), transport + N reactions (blue, *tran + N react*), transport +
1038 N reactions + plant uptake (red, *tran + N react + upta*).

1039
1040 **56.3 Reactive Transport Example 23: DOC production and export in a spatially**
1041 **explicitdistributed domain**

1042 This example showcases the application of BioRT-Flux-PIHM in a spatially
1043 explicitdistributed mode. This work has been documented with full details in [Wen et al.](#)
1044 [\(2020\)](#); [Wen et al. \(2020\)](#). Here we only introduce some key features and capabilities in
1045 the spatially explicitdistributed mode.

1046 **Model set-up.** In this example, the The Shale Hills catchment was discretized into
1047 535 prismatic land elements and 20 stream segments through PIHMgis based on the
1048 topography (Figure [10a9a](#)). The heterogeneous distributions of soil depth and solid
1049 organic carbon within the domain (Figure [10b9b-c](#)) were interpolated through ordinary
1050 kriging based on field surveys ([Andrews et al., 2011; Lin, 2006](#)); ([Andrews et al., 2011; Lin,](#)
1051 [2006](#)). Other soil and mineralogy properties such as hydraulic conductivity, van

1052 Genuchten parameters, and ion exchange capacity were ~~also~~ spatially distributed
 1053 following intensive field measurements ~~across the catchment (Jin and Brantley, 2011; Jin~~
 1054 ~~et al., 2010; Shi et al., 2013)~~(Jin and Brantley, 2011; Jin et al., 2010; Shi et al., 2013)
 1055 (criticalzone.org/shale-hills/data/).



1056
 1057 **Figure 109.** Attributes of Shale Hills in the spatially ~~explicit~~distributed mode ~~in Example 3~~: (a)
 1058 surface elevation, (b) soil depth, and (c) soil organic carbon (SOC). The surface elevation was
 1059 generated from lidar topographic data (criticalzone.org/shale-hills/data/); Soil depths and SOC
 1060 were interpolated using ordinary kriging based on field surveys ~~(Andrews et al., 2011; Lin,~~
 1061 ~~2006)~~.(Andrews et al., 2011; Lin, 2006). The SOC distribution in (c) was further simplified using
 1062 the high, uniform SOC (5% v/v) in swales and valley soils based on field survey ~~(Andrews et al.,~~
 1063 ~~2011)~~.(Andrews et al., 2011). Swales and valley floor areas were defined based on surface
 1064 elevation via field survey and a 10 m resolution digital elevation model ~~(Lin, 2006)~~.(Lin, 2006).

1066 ~~DOC was produced by the decomposition of soil organic carbon (SOC) via the~~
 1067 ~~following reaction:~~



1069 ~~The produced DOC can sorb on soils via the sorption reaction:~~



1071 ~~where $\equiv X$ and $\equiv X\text{DOC}$ represent the functional group without and with sorbed DOC,~~
 1072 ~~respectively (Rasmussen et al., 2018). For DOC production, with abundant SOC and O_2~~
 1073 ~~in shallow soils serving as electron donors and acceptors, Eq. (27) can be simplified into~~
 1074 ~~$r_{\text{DOC}} = kA f(T) f(S_w)$, where r_{DOC} is the local DOC production rate in individual grids; k is~~
 1075 ~~the kinetic rate constant of net DOC production with a value of 10^{-10} mol/m²/s (Zhi et al.,~~
 1076 ~~2019; Wieder et al., 2014); and A is the lumped “surface area” (m², $= 2.5 \times 10^{-3}$ m²/g \times g of~~
 1077 ~~SOC mass) that reflects the effective contact of water with SOC content and biomass~~
 1078 ~~(Chiou et al., 1990; Kaiser and Guggenberger, 2003; Zhi et al., 2019). The temperature~~

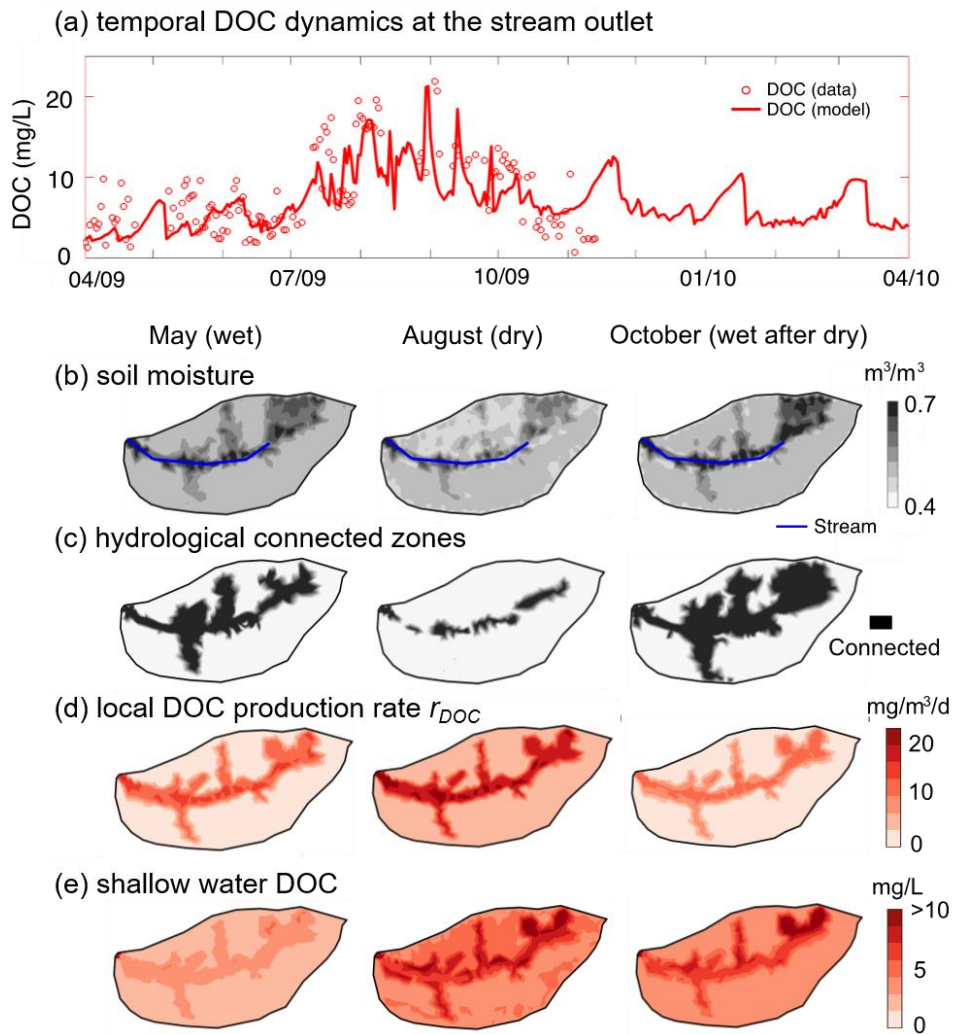
1079 ~~dependence function took the form $f(T) = 2.0^{|T-20|/10}$ while the moisture dependence~~
1080 ~~function followed $f(S_w) = (S_w)^{\pm 0}$ (Yan et al., 2018; Hamamoto et al., 2010). In DOC~~
1081 ~~sorption, equilibrium constant K_{eq} with a value of $10^{0.2}$ ($= \frac{[X][DOC]}{[X][DOC]}$) represents the~~
1082 ~~thermodynamic limit of the sorption; The sum of $[X]$ and $[XDOC]$ represents the~~
1083 ~~sorption capacity of the soil with a value ranging from 4.0×10^{-5} – 6.0×10^{-5} mol/g soil at~~
1084 ~~Shale Hills (Jin et al., 2010; Li et al., 2017a), depending on the mineralogy.~~

1085
1086 **Temporal and spatial patterns of DOC production and export.** The model outputs
1087 followed the general trend of stream DOC datameasurements (NSE = 0.55 for monthly
1088 DOC concentration; Figure 44a10a), with high values (~15 mg/L) in the dry periods (July-
1089 September). The model enabled the identification of spatial patterns and ~~the~~ hot spots of
1090 reactions. In May when soil water is relatively abundant, the valley and swales with deeper
1091 soils (Figure 44b10b) generally tended to be wetter compared to the hillslope and
1092 ridgetop, and were hydrologically connected to the stream (Figure 44b-10b, c). The
1093 distribution of local DOC production rate r_{DOC} and DOC concentration followed that of
1094 SOC (Figure 44e10c) and water content (Figure 44b10b). Low r_{DOC} in relatively dry planar
1095 hillslopes and uplands resulted in low soil water DOC. The average stream DOC (~5
1096 mg/L) reflected soil water DOC in the valley and swales.

1097 In August, the hydrologically-connected zones with high water content shrank to
1098 the vicinity of the stream and river bed. With high temperature in summer, r_{DOC} increased
1099 by 2-fold from May across the whole catchment while still exhibited the highest values in
1100 the SOC-rich regions. Soil water DOC concentration increased by a factor of 2 because
1101 the produced DOC was trapped in low soil moisture areas that were not hydrologically
1102 connected to the stream. In the north side with low water content (Figure 44b10b), the
1103 soil water DOC (~7 mg/L in average) accumulated more than the south side (~5 mg/L in
1104 average). The high shallow water DOC (~10 mg/L) in the stream vicinity dominated the
1105 stream DOC in August.

1106 In October, precipitation wetted the catchment again. The hydrologically
1107 connected zones expanded beyond swales and the valley to the upland hillslopes (Figure
1108 44e10c). The increase in hydrological connectivity zones favored the mixturemixing of
1109 shallow water DOC sourced from upland hillslopes (low DOC), swales, and valley (high

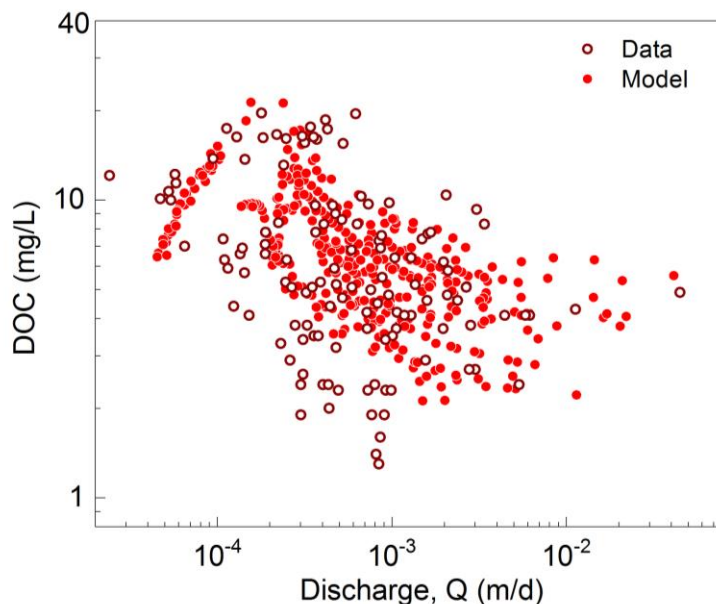
1110 DOC) into stream rather than only from the stream vicinity with high DOC in the dry
 1111 August, leading to a drop in stream DOC.



1112
 1113 **Figure 4410.** (a) Temporal dynamics of stream DOC concentration; spatial profiles of (b) shallow
 1114 soil moisture, (c) hydrologically connected zones, (d) local DOC production rates r_{DOC} and (e)
 1115 shallow water DOC concentration in May (wet), August (dry), and October (wet after dry) of 2009.
 1116 The soil DOC and r_{DOC} were high in swales and valley with relatively high shallow water and SOC
 1117 content. August had the highest shallow water DOC concentration compared to May and October,
 1118 because most DOC accumulated in zones that are disconnected to the stream.

1119
 1120 **C-Q patterns.** The DOC C-Q relationship showed a non-typical pattern with flushing first
 1121 and transitioning into a dilution pattern, with a general (an overall) C-Q slope $b = -0.23$
 1122 (Figure 4211). At low discharges ($< 1.8 \times 10^{-4}$ m/d) in the summer dry period, the stream
 1123 DOC mainly came from the organic-rich swales and valley floor zones with high soil water

1124 DOC (Figure 41e10e). With discharge increasing in wetter period (i.e., spring and fall),
1125 the contribution from planar hillslopes and uplands with lower DOC concentration
1126 increased (Figure 41e10e), leading to the dilution of stream DOC.



1127
1128 **Figure 4211.** Relationships of daily discharge (Q) with stream DOC concentration. With the
1129 increase of Q, the stream water first shifted from the dominance of groundwater with low DOC at
1130 very low discharge to the predominance of organic-rich soil water from swales and valley at
1131 intermediate discharge. As the discharge increases further, the stream water switches to the
1132 dominance of high flow with lower DOC water from planar hillslopes and uplands, resulting in a
1133 dilution C-Q pattern (modified from Wen et al., (2020)).

1135 7. Discussion

1136 The watershed biogeochemical model BioRT-Flux-PIHM brings the reactive
1137 transport modeling capabilities to the watershed scale, enabling the simulation of
1138 subsurface shallow and deep flow paths and biogeochemical reactions influenced by
1139 hydroclimatic conditions and land-surface interactions. The expanded model capability of
1140 simulating bio-mediated processes such as plant uptake, soil respiration, and microbe-
1141 mediated redox reactions enables the simulation of carbon and nutrient cycling in the
1142 shallow subsurface. The inclusion of the deep groundwater zone allows the exploration
1143 of the effects of subsurface structure on hydrological partitioning between shallow soil
1144 lateral flow and deep groundwater, and their relationships with stream discharge.
1145 Although not shown here, the model can also simulate deeper groundwater coming from

1146 regional aquifers across the outer boundary. This can be particularly useful for
1147 watersheds of higher stream orders, where a large proportion of deep water may come
1148 from nearby regional aquifers.

1149 The model presented here is complex and process-based. The computational cost
1150 of solving a spatially distributed, nonlinear, multi-component reactive transport model is
1151 high, posing challenges for the application of ensemble-based uncertainty analysis and
1152 model weighting/selection methods (Song et al., 2015). With additional reaction and
1153 transport processes, the model includes more functions (such as reaction kinetic rate
1154 laws) and parameters (e.g., reaction rate constants, surface area) than hydrological
1155 models, which have already been criticized for their complexity, equifinality, uncertainty,
1156 and data demands (Beven, 2001, 2006;Kirchner et al., 1996). These issues will persist
1157 even though reactive transport models will be constrained by additional chemical data. A
1158 major source of uncertainty in these models lies in epistemic uncertainties, i.e., the lack
1159 of specific knowledge in forcing data and details of reactivities (e.g., spatial distribution
1160 and abundance of reactive materials), on top of uncertainties related to hydrology (Beven,
1161 2000;Beven and Freer, 2001). The model's conceptual foundations also represent a
1162 major source of uncertainty.

1163 It is in this spirit of “balancing” the cost and gain that we present both spatial
1164 distributed and lumped modes for the BioRT model. Compared to the distributed version,
1165 the spatially implicit model, the spatial representation enables the exploration on requires
1166 less spatial data, is computationally inexpensive, and is relatively easy to set up. It can
1167 assess the average dynamics of the water and solute dynamics and focus on the
1168 interactions among processes without resolving spatial details. The lumped approach can
1169 also accommodate basins with low data availability, and it can be easier for students to
1170 learn to use the model. In contrast, spatially explicit representations enable the
1171 exploration of the “hot spots” (i.e.g., swales and riparian zones with high soil water DOC
1172 concentrations in Figure 44e10e) and their contribution to stream chemistry at different
1173 times. Spatial heterogeneities in watershed properties (e.g., soil types and depth,
1174 lithology, vegetation, biomass, and mineralogy) are ~~omnipresent~~ubiquitous in natural
1175 systems. ~~Yet~~However, a general understanding of the linkage between local catchment
1176 features and catchment-scale dynamics (e.g., stream concentration dynamics and solute

1177 export pattern) is ~~still~~often lacking. ~~Questions such as~~We generally do not understand
1178 how ~~the heterogeneous features affect~~spatial heterogeneity affects water flow paths,
1179 stream water chemistry, and biogeochemical reaction rates ~~remain largely unanswered.~~
1180 The spatially ~~explicit~~distributed model provides a tool to further explore these questions.
1181 Ultimately, the choice of the model complexity level depends on the research questions
1182 that the model is set to answer. At the end, we all need to balance cost and gain when
1183 deciding to use a simple or complex model, striving to be “simple but not simplistic”
1184 (Beven and Lane, 2019).

1185

1186 **68. Summary and conclusion**

1187 This paper introduces the watershed-scale biogeochemical reactive transport code
1188 BioRT (~~short for BioRT-Flux-PIHM.~~This). The code integrates processes of land-surface
1189 interactions, surface hydrology, and multi-component biogeochemical reactive transport.
1190 The new development enables the simulation of 1) biotic reactions including plant uptake,
1191 soil respiration, and microbe-mediated redox reactions ~~and plant uptake~~, and 2) surface
1192 water interactions with watergroundwater from deeper subsurface ~~zones~~that still interacts
1193 with streams. BioRT has been verified against the widely used reactive transport code
1194 CrunchTope for soil carbon, nitrogen, and phosphorus processes. The BioRT module has
1195 been applied to understand carbon, nitrogen, and weathering processes in Shale Hills in
1196 ~~central~~-Pennsylvania, Coal Creek in Colorado, and Volcán Chimborazo watershed in
1197 Andes in Ecuador. Here we showcase the modeling capability of surface-groundwater
1198 interactions, ~~transport~~ and reactive transport processes relevant to nitrate and DOC in
1199 Shale Hills in two simulation modes. One is in a spatially ~~implicit~~lumped mode using
1200 averaged properties and another is in a spatially ~~explicit~~distributed mode with
1201 consideration of spatial heterogeneity. Results show that the deep groundwater flow that
1202 interacts with the stream is primarily controlled by the hydraulic conductivity contrast
1203 between shallow and deep zone. ~~Soil~~ biogeochemical reactions in shallow soil primarily
1204 ~~determines~~determine the shallowstream water chemistry, ~~especially C, N, and biogenic~~
1205 ~~solutes~~, under high flow conditions. The spatially ~~implicit~~lumped method with two lumped
1206 grids can capture the temporal dynamics of average behavior and mass balance; the
1207 spatially ~~explicit~~distributed running mode can be used to understand the spatial dynamics

1208 and to identify “hot ~~spots~~spots” of reactions. The code can be used for biogeochemical
1209 reactive transport simulations in watersheds under diverse climate, land cover, and
1210 geology conditions.

1211
1212 **Data availability.** Field data (e.g., discharge, stream chemistry) is archived at Shale Hills
1213 data portal: <http://criticalzone.org/shale-hills/data/datasets/> or maintained at HydroShare:
1214 <https://www.hydroshare.org/group/147>.

1215
1216 **Code availability.** The current model release (BioRT-Flux-PIHM v1.0), including
1217 documentation, source code, example data, is available at GitHub repository:
1218 <https://github.com/PSUmodeling/BioRT-Flux-PIHM>.

1219
1220 **Competing interests.** The authors declare that they have no conflict of interest.

1221
1222 **Author contributions.** LL conceived the model idea and oversaw the model
1223 development. WZ coded the BioRT module, verified the code against the benchmark
1224 reactive transport model CrunchTope, and applied and tested the model at Shale Hills
1225 watershed. YS developed the deep groundwater component and integrated the BioRT-
1226 Flux-PIHM v1.0 into the MM-PIHM family. WH, LS, KS, DK, BS, and GHCN tested the
1227 code during its development and contributed ~~their~~ study cases.

1228
1229 **Acknowledgement.** We acknowledge the funding support from the Department of
1230 Energy, Subsurface Biogeochemistry Program DE-SC0020146, National Science
1231 Foundation Hydrological Sciences EAR-1758795. LS and GCN were supported by
1232 National Science Foundation Grant EAR-1759071. We appreciate data from the
1233 Susquehanna Shale Hills Critical Zone Observatory (SSHCZO) supported by National
1234 Science Foundation Grant EAR – 0725019 (C. Duffy), EAR – 1239285 (S. Brantley), and
1235 EAR – 1331726 (S. Brantley). Data were collected in Penn State's Stone Valley Forest,
1236 which is funded by the Penn State College of Agriculture Sciences, Department of
1237 Ecosystem Science and Management, and managed by the staff of the Forestlands
1238 Management Office.

1240 **References**

1241 Andrews, D. M., Lin, H., Zhu, Q., Jin, L., and Brantley, S. L.: Hot spots and hot moments of dissolved organic
1242 carbon export and soil organic carbon storage in the Shale Hills catchment, *Vadose Zone Journal*,
1243 10, 943-954, 2011.

1244 Anyah, R. O., Weaver, C. P., Miguez-Macho, G., Fan, Y., and Robock, A.: Incorporating water table
1245 dynamics in climate modeling: 3. Simulated groundwater influence on coupled land-atmosphere
1246 variability, *Journal of Geophysical Research: Atmospheres*, 113, 2008.

1247 Bai, J., Zhang, G., Zhao, Q., Lu, Q., Jia, J., Cui, B., and Liu, X.: Depth-distribution patterns and control of soil
1248 organic carbon in coastal salt marshes with different plant covers, *Sci Rep-Uk*, 6, 34835,
1249 10.1038/srep34835, 2016.

1250 Bao, C., Li, L., Shi, Y., and Duffy, C.: Understanding watershed hydrogeochemistry: 1. Development of RT-
1251 Flux-PIHM, *Water Resources Research*, 53, 2328-2345, 2017.

1252 Basu, N. B., Destouni, G., Jawitz, J. W., Thompson, S. E., Loukinova, N. V., Darracq, A., Zanardo, S., Yaeger,
1253 M., Sivapalan, M., Rinaldo, A., and Rao, P. S. C.: Nutrient loads exported from managed
1254 catchments reveal emergent biogeochemical stationarity, *Geophys. Res. Lett.*, 37,
1255 10.1029/2010GL045168, 2010.

1256 Bhatt, G., Kumar, M., and Duffy, C. J.: A tightly coupled GIS and distributed hydrologic modeling
1257 framework, *Environmental Modelling & Software*, 62, 70-84, 10.1016/j.envsoft.2014.08.003,
1258 2014.

1259 Billen, G.: Etude écologique des transformations de l'azote dans les sédiments marins, 1977.

1260 Brady, N. C., Weil, R. R., and Weil, R. R.: The nature and properties of soils, Prentice Hall Upper Saddle
1261 River, NJ, 2008.

1262 Brantley, S. L., Kubicki, J. D., and White, A. F.: Kinetics of water-rock interaction, 2008.

1263 Brantley, S. L., Lebedeva, M. I., Balashov, V. N., Singha, K., Sullivan, P. L., and Stinchcomb, G.: Toward a
1264 conceptual model relating chemical reaction fronts to water flow paths in hills, *Geomorphology*,
1265 277, 100-117, 2017.

1266 Brantley, S. L., White, T., West, N., Williams, J. Z., Forsythe, B., Shapich, D., Kaye, J., Lin, H., Shi, Y. N., Kaye,
1267 M., Herndon, E., Davis, K. J., He, Y., Eissenstat, D., Weitzman, J., DiBiase, R., Li, L., Reed, W.,
1268 Brubaker, K., and Gu, X.: Susquehanna Shale Hills Critical Zone Observatory: Shale Hills in the
1269 Context of Shaver's Creek Watershed, *Vadose Zone Journal*, 17, 1-19, ARTN 180092,
1270 10.2136/vzj2018.04.0092, 2018.

1271 Buysse, J., Smolders, E., and Merckx, R.: Modelling the uptake of nitrate by a growing plant with an
1272 adjustable root nitrate uptake capacity, *Plant and Soil*, 181, 19-23, 1996.

1273 Cai, X., Yang, Z.-L., Fisher, J., Zhang, X., Barlage, M., and Chen, F.: Integration of nitrogen dynamics into
1274 the Noah-MP land surface model v1. 1 for climate and environmental predictions, *Geoscientific
1275 Model Development (Online)*, 9, 2016.

1276 Chiou, C. T., Lee, J. F., and Boyd, S. A.: The surface area of soil organic matter, *Environmental Science &
1277 Technology*, 24, 1164-1166, 1990.

1278 Condon, L. E., Maxwell, R. M., and Gangopadhyay, S.: The impact of subsurface conceptualization on land
1279 energy fluxes, *Advances in Water Resources*, 60, 188-203, 10.1016/j.advwatres.2013.08.001,
1280 2013.

1281 Crawford, N. M., and Glass, A. D.: Molecular and physiological aspects of nitrate uptake in plants, *Trends
1282 in plant science*, 3, 389-395, 1998.

1283 Davidson, E. A., and Janssens, I. A.: Temperature sensitivity of soil carbon decomposition and feedbacks
1284 to climate change, *Nature*, 440, 165-173, 10.1038/nature04514, 2006.

1285 Davidson, E. A., Janssens, I.A.: Temperature sensitivity of soil carbon decomposition and feedbacks to
1286 climate change, *Nature*, 440, 165-173, 2006.

1287 Devienne-Barret, F., Justes, E., Machet, J., and Mary, B.: Integrated control of nitrate uptake by crop
1288 growth rate and soil nitrate availability under field conditions, *Annals of Botany*, 86, 995–1005,
1289 2000.

1290 Dingman, S. L.: *Physical hydrology*, Waveland press, 2015.

1291 Dunbabin, V. M., Diggle, A. J., Rengel, Z., and Van Hugten, R.: Modelling the interactions between water
1292 and nutrient uptake and root growth, *Plant and Soil*, 239, 19–38, 2002.

1293 Fatichi, S., Vivoni, E. R., Ogden, F. L., Ivanov, V. Y., Mirus, B., Gochis, D., Downer, C. W., Camporese, M.,
1294 Davison, J. H., Ebel, B., Jones, N., Kim, J., Mascaro, G., Niswonger, R., Restrepo, P., Rigon, R., Shen,
1295 C., Sulis, M., and Tarboton, D.: An overview of current applications, challenges, and future trends
1296 in distributed process-based models in hydrology, *Journal of Hydrology*, 537, 45–60,
1297 10.1016/j.jhydrol.2016.03.026, 2016.

1298 Fatichi, S., Manzoni, S., Or, D., and Paschalis, A.: A Mechanistic Model of Microbially Mediated Soil
1299 Biogeochemical Processes: A Reality Check, *Global Biogeochemical Cycles*, 33, 620–648,
1300 10.1029/2018gb006077, 2019.

1301 Filoso, S., Vallino, J., Hopkinson, C., Rastetter, E., and Claessens, L.: Modeling nitrogen transport in the
1302 Ipswich River Basin, Massachusetts, using a hydrological simulation program in FORTRAN (HSPF)
1303 1, *JAWRA Journal of the American Water Resources Association*, 40, 1365–1384, 2004.

1304 Fisher, J., Sitch, S., Malhi, Y., Fisher, R., Huntingford, C., and Tan, S. Y.: Carbon cost of plant nitrogen
1305 acquisition: A mechanistic, globally applicable model of plant nitrogen uptake, retranslocation,
1306 and fixation, *Global Biogeochemical Cycles*, 24, 2010.

1307 Friedlingstein, P., Cox, P., Betts, R., Bopp, L., von Bloh, W., Brovkin, V., Cadule, P., Doney, S., Eby, M., and
1308 Fung, I.: Climate-carbon cycle feedback analysis: results from the C4MIP model intercomparison,
1309 *Journal of climate*, 19, 3337–3353, 2006.

1310 Gassman, P. W., Reyes, M. R., Green, C. H., and Arnold, J. G.: The soil and water assessment tool: Historical
1311 development, applications, and future research directions, *T Asabe*, 50, 1211–1250, 2007.

1312 Gatel, L., Lauvernet, C., Carluer, N., Weill, S., Tournebize, J., and Paniconi, C.: Global evaluation and
1313 sensitivity analysis of a physically based flow and reactive transport model on a laboratory
1314 experiment, *Environmental Modelling & Software*, 113, 73–83, 10.1016/j.envsoft.2018.12.006,
1315 2019.

1316 Gleeson, T., Befus, K. M., Jasechko, S., Luijendijk, E., and Cardenas, M. B.: The global volume and
1317 distribution of modern groundwater, *Nature Geoscience*, 9, 161, 10.1038/ngeo2590
1318 <https://www.nature.com/articles/ngeo2590#supplementary-information>, 2015.

1319 Godsey, S. E., Kirchner, J. W., and Clow, D. W.: Concentration-discharge relationships reflect chemostatic
1320 characteristics of US catchments, *Hydrol. Process.*, 23, 1844–1864, 10.1002/hyp.7315, 2009.

1321 Green, T. R.: Linking climate change and groundwater, in: *Integrated groundwater management*, Springer,
1322 Cham, 97–141, 2016.

1323 Gurdak, J. J.: Groundwater: Climate-induced pumping, *Nature Geoscience*, 10, 71, 2017.

1324 Hachiya, T., and Sakakibara, H.: Interactions between nitrate and ammonium in their uptake, allocation,
1325 assimilation, and signaling in plants, *Journal of Experimental Botany*, 68, 2501–2512,
1326 10.1093/jxb/erw449, 2016.

1327 Hamamoto, S., Moldrup, P., Kawamoto, K., and Komatsu, T.: Excluded – volume expansion of Archie's law
1328 for gas and solute diffusivities and electrical and thermal conductivities in variably saturated
1329 porous media, *Water Resources Research*, 46, 2010.

1330 Han, B., Benner, S. G., and Flores, A. N.: Including Variability across Climate Change Projections in
1331 Assessing Impacts on Water Resources in an Intensively Managed Landscape, *Water*, 11, 286,
1332 2019.

1333 Hararuk, O., Smith, M. J., and Luo, Y.: Microbial models with data-driven parameters predict stronger soil
1334 carbon responses to climate change, *Glob. Chang. Biol.*, 21, 2439–2453, 10.1111/gcb.12827, 2015.

1335 Hasenmueller, E. A., Jin, L., Stinchcomb, G. E., Lin, H., Brantley, S. L., and Kaye, J. P.: Topographic controls
1336 on the depth distribution of soil CO₂ in a small temperate watershed, *Applied Geochemistry*, **63**,
1337 58-69, 2015.

1338 Hasenmueller, E. A., Gu, X., Weitzman, J. N., Adams, T. S., Stinchcomb, G. E., Eissenstat, D. M., Drohan, P.
1339 J., Brantley, S. L., and Kaye, J. P.: Weathering of rock to regolith: The activity of deep roots in
1340 bedrock fractures, *Geoderma*, **300**, 11-31, 2017.

1341 Heidari, P., Li, L., Jin, L., Williams, J. Z., and Brantley, S. L.: A reactive transport model for Marcellus shale
1342 weathering, *Geochimica et Cosmochimica Acta*, **217**, 421-440, 2017.

1343 Herndon, E. M., Dere, A. L., Sullivan, P. L., Norris, D., Reynolds, B., and Brantley, S. L.: Landscape
1344 heterogeneity drives contrasting concentration-discharge relationships in shale headwater
1345 catchments, *Hydrology and earth system sciences*, **19**, 3333-3347, 2015.

1346 Hindmarsh, A. C., Brown, P. N., Grant, K. E., Lee, S. L., Serban, R., Shumaker, D. E., and Woodward, C. S.:
1347 SUNDIALS: Suite of nonlinear and differential/algebraic equation solvers, *ACM Transactions on*
1348 *Mathematical Software (TOMS)*, **31**, 363-396, 2005.

1349 Hodges, C., Kim, H., Brantley, S. L., and Kaye, J.: Soil CO₂ and O₂ Concentrations Illuminate the Relative
1350 Importance of Weathering and Respiration to Seasonal Soil Gas Fluctuations, *Soil Science Society*
1351 *of America Journal*, **83**, 1167-1180, 2019.

1352 Jin, L., and Brantley, S. L.: Soil chemistry and shale weathering on a hillslope influenced by convergent
1353 hydrologic flow regime at the Susquehanna/Shale Hills Critical Zone Observatory, *Applied*
1354 *Geochemistry*, **26**, Supplement, S51-S56, 10.1016/j.apgeochem.2011.03.027, 2011.

1355 Jin, L. X., Ravella, R., Ketchum, B., Bierman, P. R., Heaney, P., White, T., and Brantley, S. L.: Mineral
1356 weathering and elemental transport during hillslope evolution at the Susquehanna/Shale Hills
1357 Critical Zone Observatory, *Geochim Cosmochim Ac*, **74**, 3669-3691, 10.1016/j.gca.2010.03.036,
1358 2010.

1359 Kaiser, K., and Guggenberger, G.: Mineral surfaces and soil organic matter, *European Journal of Soil*
1360 *Science*, **54**, 219-236, 10.1046/j.1365-2389.2003.00544.x, 2003.

1361 Kirchner, J. W.: A double paradox in catchment hydrology and geochemistry, *Hydrol. Process.*, **17**, 871-
1362 874, 10.1002/hyp.5108, 2003.

1363 Kuntz, B. W., Rubin, S., Berkowitz, B., and Singha, K.: Quantifying Solute Transport at the Shale Hills Critical
1364 Zone Observatory, *Vadose Zone Journal*, **10**, 843-857, 10.2136/vzj2010.0130, 2011.

1365 Lam, Q. D., Schmalz, B., and Fohrer, N.: Modelling point and diffuse source pollution of nitrate in a rural
1366 lowland catchment using the SWAT model, *Agricultural Water Management*, **97**, 317-325,
1367 10.1016/j.agwat.2009.10.004, 2010.

1368 Laroche, A. M., Gallichand, J., Lagacé, R., and Pesant, A.: Simulating atrazine transport with HSPF in an
1369 agricultural watershed, *Journal of Environmental Engineering*, **122**, 622-630, 1996.

1370 Leonard, L., and Duffy, C. J.: Essential terrestrial variable data workflows for distributed water resources
1371 modeling, *Environmental modelling & software*, **50**, 85-96, 2013.

1372 Li, L., Salehikhoo, F., Brantley, S. L., and Heidari, P.: Spatial zonation limits magnesite dissolution in porous
1373 media, *Geochimica et Cosmochimica Acta*, **126**, 555-573, 10.1016/j.gca.2013.10.051, 2014.

1374 Li, L., Bao, C., Sullivan, P. L., Brantley, S., Shi, Y., and Duffy, C.: Understanding watershed
1375 hydrogeochemistry: 2. Synchronized hydrological and geochemical processes drive stream
1376 chemostatic behavior, *Water Resources Research*, **53**, 2346-2367, 2017a.

1377 Li, L., Maher, K., Navarre-Sitchler, A., Druhan, J., Meile, C., Lawrence, C., Moore, J., Perdrial, J., Sullivan, P.,
1378 Thompson, A., Jin, L., Bolton, E. W., Brantley, S. L., Dietrich, W. E., Mayer, K. U., Steefel, C. I.,
1379 Valocchi, A., Zachara, J., Kocar, B., McIntosh, J., Tutolo, B. M., Kumar, M., Sonnenthal, E., Bao, C.,
1380 and Beisman, J.: Expanding the role of reactive transport models in critical zone processes, *Earth-*
1381 *Science Reviews*, **165**, 280-301, 10.1016/j.earscirev.2016.09.001, 2017b.

1382 Li, L., DiBiase, R. A., Del Vecchio, J., Marcon, V., Hoagland, B., Xiao, D., Wayman, C., Tang, Q., He, Y.,
1383 Silverhart, P., Szink, I., Forsythe, B., Williams, J. Z., Shapich, D., Mount, G. J., Kaye, J., Guo, L., Lin,
1384 H., Eissenstat, D., Dere, A., Brubaker, K., Kaye, M., Davis, K. J., Russo, T., and Brantley, S. L.: The
1385 Effect of Lithology and Agriculture at the Susquehanna Shale Hills Critical Zone Observatory,
1386 *Vadose Zone Journal*, 17, 10.2136/vzj2018.03.0063, 2018.

1387 Li, L.: Watershed reactive transport, *Reviews in Mineralogy and Geochemistry*, 85, 381-418, 2019.

1388 Lin, H.: Temporal stability of soil moisture spatial pattern and subsurface preferential flow pathways in
1389 the shale hills catchment, *Vadose Zone J*, 5, 317-340, 10.2136/vzj2005.0058, 2006.

1390 Maavara, T., Lauerwald, R., Laruelle, G. G., Akbarzadeh, Z., Bouskill, N. J., Van Cappellen, P., and Regnier,
1391 P.: Nitrous oxide emissions from inland waters: Are IPCC estimates too high?, *Global Change
1392 Biology*, 0, doi:10.1111/gcb.14504, 2018.

1393 MacQuarrie, K. T. B., and Mayer, K. U.: Reactive transport modeling in fractured rock: A state-of-the-
1394 science review, *Earth Science Reviews*, 72, 189-227, 10.1016/j.earscirev.2005.07.003, 2005.

1395 Marin-Spiotta, E., Silver, W. L., Swanston, C. W., and Ostertag, R.: Soil organic matter dynamics during 80
1396 years of reforestation of tropical pastures, *Global Change Biology*, 15, 1584-1597, 10.1111/j.1365-
1397 2486.2008.01805.x, 2009.

1398 Maxwell, R. M., Lundquist, J. K., Mirocha, J. D., Smith, S. G., Woodward, C. S., and Tompson, A. F.:
1399 Development of a coupled groundwater-atmosphere model, *Monthly Weather Review*, 139, 96-
1400 116, 2011.

1401 Mayer, K. U., Frind, E. O., and Blowes, D. W.: Multicomponent reactive transport modeling in variably
1402 saturated porous media using a generalized formulation for kinetically controlled reactions,
1403 *Water Resources Research*, 38, 13-11-13-21, 10.1029/2001wr000862, 2002.

1404 Miller, M. P., Tesoriero, A. J., Hood, K., Terziotti, S., and Wolock, D. M.: Estimating Discharge and Nonpoint
1405 Source Nitrate Loading to Streams From Three End-Member Pathways Using High-Frequency
1406 Water Quality Data, *Water Resources Research*, 53, 10201-10216, 10.1002/2017wr021654, 2017.

1407 Miller, M. P., Capel, P. D., Garcia, A. M., and Ator, S. W.: Response of Nitrogen Loading to the Chesapeake
1408 Bay to Source Reduction and Land Use Change Scenarios: A SPARROW - Informed Analysis,
1409 *JAWRA Journal of the American Water Resources Association*, 56, 100-112, 2020.

1410 Moatar, F., Abbott, B. W., Minaudo, C., Curie, F., and Pinay, G.: Elemental properties, hydrology, and
1411 biology interact to shape concentration - discharge curves for carbon, nutrients, sediment, and
1412 major ions, *Water Resources Research*, 53, 1270-1287, 2017.

1413 Monod, J.: The growth of bacterial cultures, *Annual review of microbiology*, 3, 371-394, 1949.

1414 Moriasi, D. N., Gowda, P. H., Arnold, J. G., Mulla, D. J., Ale, S., and Steiner, J. L.: Modeling the impact of
1415 nitrogen fertilizer application and tile drain configuration on nitrate leaching using SWAT,
1416 *Agricultural Water Management*, 130, 36-43, 10.1016/j.agwat.2013.08.003, 2013.

1417 Musolff, A., Schmidt, C., Selle, B., and Fleckenstein, J. H.: Catchment controls on solute export, *Adv. Water
1418 Resour.*, 86, 133-146, 10.1016/j.advwatres.2015.09.026, 2015.

1419 Neitsch, S. L., Arnold, J. G., Kiniry, J. R., and Williams, J. R.: Soil and water assessment tool theoretical
1420 documentation version 2009, Texas Water Resources Institute, 2011.

1421 Niu, J., and Phanikumar, M. S.: Modeling watershed-scale solute transport using an integrated, process-
1422 based hydrologic model with applications to bacterial fate and transport, *Journal of Hydrology*,
1423 529, 35-48, 10.1016/j.jhydrol.2015.07.013, 2015.

1424 Ostle, N. J., Smith, P., Fisher, R., Woodward, F. I., Fisher, J. B., Smith, J. U., Galbraith, D., Levy, P., Meir, P.,
1425 McNamara, N. P., and Bardgett, R. D.: Integrating plant-soil interactions into global carbon cycle
1426 models, *Journal of Ecology*, 97, 851-863, 10.1111/j.1365-2745.2009.01547.x, 2009.

1427 Ottoy, S., Elsen, A., Van De Vreken, P., Gobin, A., Merckx, R., Hermy, M., and Van Orshoven, J.: An
1428 exponential change decline function to estimate soil organic carbon stocks and their changes from
1429 topsoil measurements, *European Journal of Soil Science*, 67, 816-826, 2016.

1430 Porporato, A., D'odorico, P., Laio, F., and Rodriguez-Iturbe, I.: Hydrologic controls on soil carbon and
1431 nitrogen cycles. I. Modeling scheme, *Advances in water resources*, 26, 45–58, 2003.

1432 Qiu, H., Niu, J., and Hu, B. X.: Quantifying the integrated water and carbon cycle in a data-limited karst
1433 basin using a process-based hydrologic model, *Environmental Earth Sciences*, 78, 328, 2019.

1434 Qu, Y., and Duffy, C. J.: A semidiscrete finite volume formulation for multiprocess watershed simulation,
1435 *Water Resour. Res.*, 43, W08419, 10.1029/2006wr005752, 2007.

1436 Rasmussen, C., Heckman, K., Wieder, W. R., Keiluweit, M., Lawrence, C. R., Berhe, A. A., Blankinship, J. C.,
1437 Crow, S. E., Druhan, J. L., Hicks-Pries, C. E., Marin-Spiotta, E., Plante, A. F., Schädel, C., Schimel, J.
1438 P., Sierra, C. A., Thompson, A., and Wagai, R.: Beyond clay: towards an improved set of variables
1439 for predicting soil organic matter content, *Biogeochemistry*, 137, 297–306, 10.1007/s10533-018-
1440 0424-3, 2018.

1441 Regnier, P., and Steefel, C. I.: A high-resolution estimate of the inorganic nitrogen flux from the Scheldt
1442 estuary to the coastal North-Sea during a nitrogen-limited algal bloom, spring 1995, *Geochimica
1443 et Cosmochimica Acta*, 63, 1359–1374, 10.1016/s0016-7037(99)00034-4, 1999.

1444 Rutherford, D. W., Chiou, C. T., and Kile, D. E.: Influence of soil organic matter composition on the partition
1445 of organic compounds, *Environmental science & technology*, 26, 336–340, 1992.

1446 Saha, D., Rau, B. M., Kaye, J. P., Montes, F., Adler, P. R., and Kemanian, A. R.: Landscape control of nitrous
1447 oxide emissions during the transition from conservation reserve program to perennial grasses for
1448 bioenergy, *GCB Bioenergy*, 9, 783–795, 10.1111/gcbb.12395, 2017.

1449 Scudeler, C., Pangle, L., Pasetto, D., Niu, G.-Y., Volkmann, T., Paniconi, C., Putti, M., and Troch, P.:
1450 Multiresponse modeling of variably saturated flow and isotope tracer transport for a hillslope
1451 experiment at the Landscape Evolution Observatory, *Hydrology and Earth System Sciences*, 20,
1452 4061–4078, 2016.

1453 Sebestyén, S. D., Ross, D. S., Shanley, J. B., Elliott, E. M., Kendall, C., Campbell, J. L., Dail, D. B., Fernandez,
1454 I. J., Goodale, C. L., and Lawrence, G. B.: Unprocessed Atmospheric Nitrate in Waters of the
1455 Northern Forest Region in the US and Canada, *Environmental science & technology*, 53, 3620–
1456 3633, 2019.

1457 Seibert, J., Grabs, T., Köhler, S., Laudon, H., Winterdahl, M., and Bishop, K.: Linking soil and stream water
1458 chemistry based on a Riparian Flow Concentration Integration Model, *Hydrol. Earth Syst. Sci.*, 13,
1459 2287–2297, 10.5194/hess-13-2287-2009, 2009.

1460 Shi, Y.: Development of a land surface hydrologic modeling and data-assimilation system for the study of
1461 subsurface-land surface interaction, 2012.

1462 Shi, Y., Davis, K. J., Duffy, C. J., and Yu, X.: Development of a coupled land surface hydrologic model and
1463 evaluation at a critical zone observatory, *Journal of Hydrometeorology*, 14, 1401–1420, 2013.

1464 Shi, Y., Eissenstat, D. M., He, Y., and Davis, K. J.: Using a spatially distributed hydrologic biogeochemistry
1465 model with a nitrogen transport module to study the spatial variation of carbon processes in a
1466 Critical Zone Observatory, *Ecological Modelling*, 380, 8–21, 2018.

1467 Skamarock, W., and Klemp, J.: A Description of the Advanced Research WRF Model Version 4. Near
1468 Technical Notes, No. NCAR/TN-556+STR, 2019.

1469 Steefel, C., Appelo, C., Arora, B., Jacques, D., Kalbacher, T., Kolditz, O., Lagneau, V., Lichtner, P., Mayer, K.
1470 U., and Meeussen, J.: Reactive transport codes for subsurface environmental simulation,
1471 *Computational Geosciences*, 19, 445–478, 2015.

1472 Steefel, C. I., and Lasaga, A. C.: A coupled model for transport of multiple chemical species and kinetic
1473 precipitation/dissolution reactions with application to reactive flow in single-phase hydrothermal
1474 systems, *American Journal of science*, 294, 529–592, 1994.

1475 Steimke, A. L., Han, B., Brandt, J. S., and Flores, A. N.: Climate change and curtailment: Evaluating water
1476 management practices in the context of changing runoff regimes in a snowmelt-dominated basin,
1477 *Water*, 10, 1490, 2018.

1478 Taylor, R. G., Scanlon, B., Döll, P., Rodell, M., Van Beek, R., Wada, Y., Longuevergne, L., Leblanc, M.,
1479 Famiglietti, J. S., and Edmunds, M.: Ground water and climate change, *Nature climate change*, 3,
1480 322, 2013.

1481 Thornton, P. E., Doney, S. C., Lindsay, K., Moore, J. K., Mahowald, N., Randerson, J. T., Fung, I., Lamarque,
1482 J. F., Feddes, J. J., and Lee, Y. H.: Carbon-nitrogen interactions regulate climate-carbon cycle
1483 feedbacks: results from an atmosphere-ocean general circulation model, *Biogeosciences*, 6, 2099-
1484 2120, 10.5194/bg-6-2099-2009, 2009.

1485 Todd, D. K., and Mays, L. W.: *Groundwater Hydrology*, Welly Inte, 2005.

1486 Trumbore, S. E.: Comparison of carbon dynamics in tropical and temperate soils using radiocarbon
1487 measurements, *Global Biogeochemical Cycles*, 7, 275-290, 10.1029/93GB00468, 1993.

1488 van der Velde, Y., de Rooij, G. H., Rozemeijer, J. C., van Geer, F. C., and Broers, H. P.: Nitrate response of
1489 a lowland catchment: On the relation between stream concentration and travel time distribution
1490 dynamics, *Water Resources Research*, 46, 10.1029/2010wr009105, 2010.

1491 van der Velde, Y., Vercauteren, N., Jaramillo, F., Dekker, S. C., Destouni, G., and Lyon, S. W.: Exploring
1492 hydroclimatic change disparity via the Budyko framework, *Hydrological Processes*, 28, 4110-4118,
1493 10.1002/hyp.9949, 2014.

1494 Weiler, M., and McDonnell, J. R. J.: Testing nutrient flushing hypotheses at the hillslope scale: A virtual
1495 experiment approach, *J. Hydrol.*, 319, 339-356, 10.1016/j.jhydrol.2005.06.040, 2006.

1496 Weitzman, J. N., and Kaye, J. P.: Nitrogen Budget and Topographic Controls on Nitrous Oxide in a Shale-
1497 Based Watershed, *Journal of Geophysical Research: Biogeosciences*, 123, 1888-1908, 2018.

1498 Wen, H., Perdrial, J., Bernal, S., Abbott, B. W., Dupas, R., Godsey, S. E., Harpold, A., Rizzo, D., Underwood,
1499 K., and Adler, T.: Temperature controls production but hydrology controls export of dissolved
1500 organic carbon at the catchment scale, 24, 945-966, 2020.

1501 Wieder, W. R., Grandy, A. S., Kallenbach, C. M., and Bonan, G. B.: Integrating microbial physiology and
1502 physio-chemical principles in soils with the Microbial Mineral Carbon Stabilization (MIMICS)
1503 model, *Biogeosciences*, 11, 3899-3917, 10.5194/bg-11-3899-2014, 2014.

1504 Wieder, W. R., Allison, S. D., Davidson, E. A., Georgiou, K., Hararuk, O., He, Y., Hopkins, F., Luo, Y., Smith,
1505 M. J., and Sulman, B.: Explicitly representing soil microbial processes in Earth system models,
1506 *Global Biogeochemical Cycles*, 29, 1782-1800, 2015.

1507 Winter, T., Harvey, J., Franke, O., and Alley, W.: Natural processes of ground water and surface water
1508 interaction, *Ground Water and Surface Water: A Single Resource*, US Geological Survey Circular,
1509 1139, 2-50, 1998.

1510 Yan, Z. F., Bond-Lamberty, B., Todd-Brown, K. E., Bailey, V. L., Li, S. L., Liu, C. Q., and Liu, C. X.: A moisture
1511 function of soil heterotrophic respiration that incorporates microscale processes, *Nature*
1512 *Communications*, 9, 10.1038/s41467-018-04971-6, 2018.

1513 Zarnetske, J. P., Bouda, M., Abbott, B. W., Saiers, J., and Raymond, P. A.: Generality of hydrologic transport
1514 limitation of watershed organic carbon flux across ecoregions of the United States, *Geophysical*
1515 *Research Letters*, 45, 11,702-711,711, 2018.

1516 Zhi, W., Li, L., Dong, W. M., Brown, W., Kaye, J., Steefel, C., and Williams, K. H.: Distinct Source Water
1517 Chemistry Shapes Contrasting Concentration-Discharge Patterns, *Water Resources Research*, 55, 4233-
1518 4251, 10.1029/2018wr024257, 2019.

1519 Andrews, D. M., Lin, H., Zhu, Q., Jin, L., and Brantley, S. L.: Hot spots
1520 and hot moments of dissolved organic carbon export and soil organic carbon storage in the Shale Hills
1521 catchment, *Vadose Zone Journal*, 10, 943-954, 2011.

1522 Anyah, R. O., Weaver, C. P., Miguez - Macho, G., Fan, Y., and Robock, A.: Incorporating water table
1523 dynamics in climate modeling: 3. Simulated groundwater influence on coupled land - atmosphere
1524 variability, *Journal of Geophysical Research: Atmospheres*, 113, 2008.

1524 [Bai, J., Zhang, G., Zhao, Q., Lu, Q., Jia, J., Cui, B., and Liu, X.: Depth-distribution patterns and control of soil](#)
1525 [organic carbon in coastal salt marshes with different plant covers, *Sci Rep-UK*, 6, 34835,](#)
1526 [10.1038/srep34835, 2016.](#)

1527 [Bailey, R., Rathjens, H., Bieger, K., Chaubey, I., and Arnold, J.: SWATMOD-Prep: Graphical User Interface](#)
1528 [for Preparing Coupled SWAT-MODFLOW Simulations, *JAWRA Journal of the American Water Resources*](#)
1529 [Association, 53, 400-410, <https://doi.org/10.1111/1752-1688.12502>, 2017.](#)

1530 [Bao, C., Wu, H., Li, L., Newcomer, D., Long, P. E., and Williams, K. H.: Uranium Bioreduction Rates across](#)
1531 [Scales: Biogeochemical Hot Moments and Hot Spots during a Biostimulation Experiment at Rifle, Colorado,](#)
1532 [Environmental Science & Technology, 48, 10116-10127, 10.1021/es501060d, 2014.](#)

1533 [Bao, C., Li, L., Shi, Y., and Duffy, C.: Understanding watershed hydrogeochemistry: 1. Development of RT -](#)
1534 [Flux - PIHM, *Water Resources Research*, 53, 2328-2345, 2017.](#)

1535 [Basu, N. B., Destouni, G., Jawitz, J. W., Thompson, S. E., Loukinova, N. V., Darracq, A., Zanardo, S., Yaeger,](#)
1536 [M., Sivapalan, M., Rinaldo, A., and Rao, P. S. C.: Nutrient loads exported from managed catchments reveal](#)
1537 [emergent biogeochemical stationarity, *Geophys. Res. Lett.*, 37, 10.1029/2010GL045168, 2010.](#)

1538 [Beven, K.: How far can we go in distributed hydrological modelling?, *Hydrol. Earth Syst. Sci.*, 5, 1-12,](#)
1539 [10.5194/hess-5-1-2001, 2001.](#)

1540 [Beven, K., and Freer, J.: Equifinality, data assimilation, and uncertainty estimation in mechanistic](#)
1541 [modelling of complex environmental systems using the GLUE methodology, *Journal of Hydrology*, 249,](#)
1542 [11-29, 10.1016/s0022-1694\(01\)00421-8, 2001.](#)

1543 [Beven, K.: A manifesto for the equifinality thesis, *Journal of Hydrology*, 320, 18-36,](#)
1544 [10.1016/j.jhydrol.2005.07.007, 2006.](#)

1545 [Beven, K., and Lane, S.: Invalidation of Models and Fitness-for-Purpose: A Rejectionist Approach, in:](#)
1546 [Computer Simulation Validation: Fundamental Concepts, Methodological Frameworks, and Philosophical](#)
1547 [Perspectives, edited by: Beisbart, C., and Saam, N. J., Springer International Publishing, Cham, 145-171,](#)
1548 [2019.](#)

1549 [Beven, K. J.: Uniqueness of place and process representations in hydrological modelling, *Hydrol. Earth*](#)
1550 [Syst. Sci.](#), 4, 203-213, 10.5194/hess-4-203-2000, 2000.

1551 [Bhatt, G., Kumar, M., and Duffy, C. J.: A tightly coupled GIS and distributed hydrologic modeling](#)
1552 [framework, *Environmental Modelling & Software*, 62, 70-84,](#)
1553 [http://dx.doi.org/10.1016/j.envsoft.2014.08.003, 2014.](#)

1554 [Billen, G.: Etude écologique des transformations de l'azote dans les sédiments marins, 1977.](#)

1555 [Bracho, R., Natali, S., Pegoraro, E., Crummer, K. G., Schädel, C., Celis, G., Hale, L., Wu, L., Yin, H., and Tiedje,](#)
1556 [J. M.: Temperature sensitivity of organic matter decomposition of permafrost-region soils during](#)
1557 [laboratory incubations, *Soil Biology and Biochemistry*, 97, 1-14, 2016.](#)

1558 [Brantley, S. L., Kubicki, J. D., and White, A. F.: Kinetics of water-rock interaction, 2008.](#)

1559 [Brantley, S. L., White, T., West, N., Williams, J. Z., Forsythe, B., Shapich, D., Kaye, J., Lin, H., Shi, Y. N., Kaye,](#)
1560 [M., Herndon, E., Davis, K. J., He, Y., Eissenstat, D., Weitzman, J., DiBiase, R., Li, L., Reed, W., Brubaker, K.,](#)
1561 [and Gu, X.: Susquehanna Shale Hills Critical Zone Observatory: Shale Hills in the Context of Shaver's Creek](#)
1562 [Watershed, *Vadose Zone Journal*, 17, 1-19, ARTN 180092](#)
1563 [10.2136/vzj2018.04.0092, 2018.](#)

1564 [Brooks, P. D., Chorover, J., Fan, Y., Godsey, S. E., Maxwell, R. M., McNamara, J. P., and Tague, C.:](#)
1565 [Hydrological partitioning in the critical zone: Recent advances and opportunities for developing](#)
1566 [transferable understanding of water cycle dynamics, *Water Resources Research*, 51, 6973-6987,](#)
1567 [https://doi.org/10.1002/2015WR017039, 2015.](#)

1568 [Buljovic, Z., and Engels, C.: Nitrate uptake ability by maize roots during and after drought stress, *Plant*](#)
1569 [and Soil](#), 229, 125-135, 2001.

1570 [Buysse, J., Smolders, E., and Merckx, R.: Modelling the uptake of nitrate by a growing plant with an](#)
1571 [adjustable root nitrate uptake capacity, *Plant and Soil*, 181, 19-23, 1996.](#)

1572 [Cai, X., Yang, Z.-L., Fisher, J., Zhang, X., Barlage, M., and Chen, F.: Integration of nitrogen dynamics into](#)
1573 [the Noah-MP land surface model v1. 1 for climate and environmental predictions, *Geoscientific Model*](#)
1574 [Development \(Online\), 9, 2016.](#)

1575 [Chiou, C. T., Lee, J. F., and Boyd, S. A.: The surface area of soil organic matter, *Environmental Science &*](#)
1576 [Technology, 24, 1164-1166, 1990.](#)

1577 [Condon, L. E., Maxwell, R. M., and Gangopadhyay, S.: The impact of subsurface conceptualization on land](#)
1578 [energy fluxes, *Advances in Water Resources*, 60, 188-203,](#)
1579 <https://doi.org/10.1016/j.advwatres.2013.08.001>, 2013.

1580 [Crawford, N. M., and Glass, A. D.: Molecular and physiological aspects of nitrate uptake in plants, *Trends*](#)
1581 [in plant science, 3, 389-395, 1998.](#)

1582 [Davidson, E. A., and Janssens, I. A.: Temperature sensitivity of soil carbon decomposition and feedbacks](#)
1583 [to climate change, *Nature*, 440, 165-173, 10.1038/nature04514, 2006.](#)

1584 [Davidson, E. A., Janssens, I. A., and Luo, Y.: On the variability of respiration in terrestrial ecosystems:](#)
1585 [moving beyond Q10, *Global Change Biology*, 12, 154-164, 2006.](#)

1586 [Davidson, E. A., Janssens, I.A.: Temperature sensitivity of soil carbon decomposition and feedbacks to](#)
1587 [climate change, *Nature*, 440, 165-173, 2006.](#)

1588 [Deviene-Barret, F., Justes, E., Machel, J., and Mary, B.: Integrated control of nitrate uptake by crop](#)
1589 [growth rate and soil nitrate availability under field conditions, *Annals of Botany*, 86, 995-1005, 2000.](#)

1590 [Di Capua, F., Pirozzi, F., Lens, P. N. L., and Esposito, G.: Electron donors for autotrophic denitrification,](#)
1591 [Chemical Engineering Journal, 362, 922-937, https://doi.org/10.1016/j.cej.2019.01.069, 2019.](#)

1592 [Dingman, S. L.: Physical hydrology, Waveland press, 2015.](#)

1593 [Dunbabin, V. M., Diggle, A. J., Rengel, Z., and Van Hugten, R.: Modelling the interactions between water](#)
1594 [and nutrient uptake and root growth, *Plant and Soil*, 239, 19-38, 2002.](#)

1595 [Edwards, P. J., Williard, K. W. J., and Schoonover, J. E.: Fundamentals of Watershed Hydrology, *Journal of*](#)
1596 [Contemporary Water Research & Education, 154, 3-20, 10.1111/j.1936-704X.2015.03185.x, 2015.](#)

1597 [Fatichi, S., Vivoni, E. R., Ogden, F. L., Ivanov, V. Y., Mirus, B., Gochis, D., Downer, C. W., Camporese, M.,](#)
1598 [Davison, J. H., Ebel, B., Jones, N., Kim, J., Mascaro, G., Niswonger, R., Restrepo, P., Rigon, R., Shen, C., Sulis,](#)
1599 [M., and Tarboton, D.: An overview of current applications, challenges, and future trends in distributed](#)
1600 [process-based models in hydrology, *Journal of Hydrology*, 537, 45-60,](#)
1601 <https://doi.org/10.1016/j.jhydrol.2016.03.026>, 2016.

1602 [Fatichi, S., Manzoni, S., Or, D., and Paschalis, A.: A Mechanistic Model of Microbially Mediated Soil](#)
1603 [Biogeochemical Processes: A Reality Check, *Global Biogeochemical Cycles*, 33, 620-648,](#)
1604 <10.1029/2018gb006077>, 2019.

1605 [Fisher, J., Sitch, S., Malhi, Y., Fisher, R., Huntingford, C., and Tan, S. Y.: Carbon cost of plant nitrogen](#)
1606 [acquisition: A mechanistic, globally applicable model of plant nitrogen uptake, retranslocation, and](#)
1607 [fixation, *Global Biogeochemical Cycles*, 24, 2010.](#)

1608 [Friedlingstein, P., Cox, P., Betts, R., Bopp, L., von Bloh, W., Brovkin, V., Cadule, P., Doney, S., Eby, M., and](#)
1609 [Fung, I.: Climate-carbon cycle feedback analysis: results from the C4MIP model intercomparison, *Journal*](#)
1610 [of climate, 19, 3337-3353, 2006.](#)

1611 [Gassman, P. W., Reyes, M. R., Green, C. H., and Arnold, J. G.: The soil and water assessment tool: Historical](#)
1612 [development, applications, and future research directions, *T Asabe*, 50, 1211-1250, 2007.](#)

1613 [Gatel, L., Lauvernet, C., Carluer, N., Weill, S., Tournebize, J., and Paniconi, C.: Global evaluation and](#)
1614 [sensitivity analysis of a physically based flow and reactive transport model on a laboratory experiment,](#)
1615 [Environmental Modelling & Software, 113, 73-83, https://doi.org/10.1016/j.envsoft.2018.12.006, 2019.](#)

1616 [Gleeson, T., Befus, K. M., Jasechko, S., Luijendijk, E., and Cardenas, M. B.: The global volume and](#)
1617 [distribution of modern groundwater, *Nature Geoscience*, 9, 161, 10.1038/ngeo2590](#)

1618 <https://www.nature.com/articles/ngeo2590#supplementary-information>, 2015.

1619 [Godsey, S. E., Kirchner, J. W., and Clow, D. W.: Concentration–discharge relationships reflect chemostatic](#)

1620 [characteristics of US catchments, *Hydrol. Process.*, 23, 1844-1864, 10.1002/hyp.7315, 2009.](#)

1621 [Godsey, S. E., Hartmann, J., and Kirchner, J. W.: Catchment chemostasis revisited: Water quality responds](#)

1622 [differently to variations in weather and climate, *Hydrological Processes*, 33, 3056-3069,](#)

1623 <https://doi.org/10.1002/hyp.13554>, 2019.

1624 [Grathwohl, P., Rügner, H., Wöhling, T., Osenbrück, K., Schwientek, M., Gayler, S., Wollschläger, U., Selle,](#)

1625 [B., Pause, M., and Delfs, J.-O.: Catchments as reactors: a comprehensive approach for water fluxes and](#)

1626 [solute turnover, *Environmental earth sciences*, 69, 317-333, 2013.](#)

1627 [Green, T. R.: Linking climate change and groundwater, in: *Integrated groundwater management*, Springer,](#)

1628 [Cham, 97-141, 2016.](#)

1629 [Gurdak, J. J.: Groundwater: Climate-induced pumping, *Nature Geoscience*, 10, 71, 2017.](#)

1630 [Hachiya, T., and Sakakibara, H.: Interactions between nitrate and ammonium in their uptake, allocation,](#)

1631 [assimilation, and signaling in plants, *Journal of Experimental Botany*, 68, 2501-2512, 10.1093/jxb/erw449,](#)

1632 [2016.](#)

1633 [Hamamoto, S., Moldrup, P., Kawamoto, K., and Komatsu, T.: Excluded - volume expansion of Archie's law](#)

1634 [for gas and solute diffusivities and electrical and thermal conductivities in variably saturated porous](#)

1635 [media, *Water Resources Research*, 46, 2010.](#)

1636 [Han, B., Benner, S. G., and Flores, A. N.: Including Variability across Climate Change Projections in](#)

1637 [Assessing Impacts on Water Resources in an Intensively Managed Landscape, *Water*, 11, 286, 2019.](#)

1638 [Hararuk, O., Smith, M. J., and Luo, Y.: Microbial models with data-driven parameters predict stronger soil](#)

1639 [carbon responses to climate change, *Glob. Chang. Biol.*, 21, 2439-2453, 10.1111/gcb.12827, 2015.](#)

1640 [HARTLEY, I. P., HEINEMEYER, A., and INESON, P.: Effects of three years of soil warming and shading on the](#)

1641 [rate of soil respiration: substrate availability and not thermal acclimation mediates observed response,](#)

1642 [Global Change Biology, 13, 1761-1770, https://doi.org/10.1111/j.1365-2486.2007.01373.x, 2007.](#)

1643 [Hartmann, J., Lauerwald, R., and Moosdorf, N.: A brief overview of the GLObal River CHEmistry Database,](#)

1644 [GLORICH, *Procedia Earth and Planetary Science*, 10, 23-27, 2014.](#)

1645 [Hasenmueller, E. A., Jin, L., Stinchcomb, G. E., Lin, H., Brantley, S. L., and Kaye, J. P.: Topographic controls](#)

1646 [on the depth distribution of soil CO₂ in a small temperate watershed, *Applied Geochemistry*, 63, 58-69,](#)

1647 [2015.](#)

1648 [Hasenmueller, E. A., Gu, X., Weitzman, J. N., Adams, T. S., Stinchcomb, G. E., Eissenstat, D. M., Drohan, P.](#)

1649 [J., Brantley, S. L., and Kaye, J. P.: Weathering of rock to regolith: The activity of deep roots in bedrock](#)

1650 [fractures, *Geoderma*, 300, 11-31, 2017.](#)

1651 [Heidari, P., Li, L., Jin, L., Williams, J. Z., and Brantley, S. L.: A reactive transport model for Marcellus shale](#)

1652 [weathering, *Geochimica et Cosmochimica Acta*, 217, 421-440, 2017.](#)

1653 [Herndon, E. M., Dere, A. L., Sullivan, P. L., Norris, D., Reynolds, B., and Brantley, S. L.: Landscape](#)

1654 [heterogeneity drives contrasting concentration–discharge relationships in shale headwater catchments,](#)

1655 [Hydrology and earth system sciences, 19, 3333-3347, 2015.](#)

1656 [Hindmarsh, A. C., Brown, P. N., Grant, K. E., Lee, S. L., Serban, R., Shumaker, D. E., and Woodward, C. S.:](#)

1657 [SUNDIALS: Suite of nonlinear and differential/algebraic equation solvers, *ACM Transactions on*](#)

1658 [Mathematical Software \(TOMS\), 31, 363-396, 2005.](#)

1659 [Hodges, C., Kim, H., Brantley, S. L., and Kaye, J.: Soil CO₂ and O₂ Concentrations Illuminate the Relative](#)

1660 [Importance of Weathering and Respiration to Seasonal Soil Gas Fluctuations, *Soil Science Society of*](#)

1661 [America Journal, 83, 1167-1180, 2019.](#)

1662 [Hubbard, S. S., Williams, K. H., Agarwal, D., Banfield, J., Beller, H., Bouskill, N., Brodie, E., Carroll, R.,](#)

1663 [Dafflon, B., and Dwivedi, D.: The East River, Colorado, Watershed: A mountainous community testbed for](#)

1664 [improving predictive understanding of multiscale hydrological–biogeochemical dynamics, *Vadose Zone*](#)

1665 [Journal, 17, 2018.](#)

1666 [Husic, A.: Numerical modeling and isotope tracers to investigate karst biogeochemistry and transport](#)
1667 [processes, 2018.](#)

1668 [Jin, L., and Brantley, S. L.: Soil chemistry and shale weathering on a hillslope influenced by convergent](#)
1669 [hydrologic flow regime at the Susquehanna/Shale Hills Critical Zone Observatory, Applied Geochemistry,](#)
1670 [26, Supplement, S51-S56, <http://dx.doi.org/10.1016/j.apgeochem.2011.03.027>, 2011.](#)

1671 [Jin, L. X., Ravella, R., Ketchum, B., Bierman, P. R., Heaney, P., White, T., and Brantley, S. L.: Mineral](#)
1672 [weathering and elemental transport during hillslope evolution at the Susquehanna/Shale Hills Critical](#)
1673 [Zone Observatory, Geochim Cosmochim Acta, 74, 3669-3691, \[10.1016/j.gca.2010.03.036\]\(https://doi.org/10.1016/j.gca.2010.03.036\), 2010.](#)

1674 [Keune, J., Gasper, F., Goergen, K., Hense, A., Shrestha, P., Sulis, M., and Kollet, S.: Studying the influence](#)
1675 [of groundwater representations on land surface-atmosphere feedbacks during the European heat wave](#)
1676 [in 2003, Journal of Geophysical Research: Atmospheres, 121, 31301-313325,](#)
1677 <https://doi.org/10.1002/2016JD025426>, 2016.

1678 [Kirchner, J. W., Hooper, R. P., Kendall, C., Neal, C., and Leavesley, G.: Testing and validating environmental](#)
1679 [models, Science of the Total Environment, 183, 33-47, \[10.1016/0048-9697\\(95\\)04971-1\]\(https://doi.org/10.1016/0048-9697\(95\)04971-1\), 1996.](#)

1680 [Kirchner, J. W.: A double paradox in catchment hydrology and geochemistry, Hydrol. Process., 17, 871-](#)
1681 [874, \[10.1002/hyp.5108\]\(https://doi.org/10.1002/hyp.5108\), 2003.](#)

1682 [Kuntz, B. W., Rubin, S., Berkowitz, B., and Singha, K.: Quantifying Solute Transport at the Shale Hills Critical](#)
1683 [Zone Observatory, Vadose Zone Journal, 10, 843-857, \[10.2136/vzj2010.0130\]\(https://doi.org/10.2136/vzj2010.0130\), 2011.](#)

1684 [Lam, Q. D., Schmalz, B., and Fohrer, N.: Modelling point and diffuse source pollution of nitrate in a rural](#)
1685 [lowland catchment using the SWAT model, Agricultural Water Management, 97, 317-325,](#)
1686 <https://doi.org/10.1016/j.agwat.2009.10.004>, 2010.

1687 [Leonard, L., and Duffy, C. J.: Essential terrestrial variable data workflows for distributed water resources](#)
1688 [modeling, Environmental Modelling & Software, 50, 85-96, 2013.](#)

1689 [Li, L., Salehikhoo, F., Brantley, S. L., and Heidari, P.: Spatial zonation limits magnesite dissolution in porous](#)
1690 [media, Geochimica et Cosmochimica Acta, 126, 555-573, \[10.1016/j.gca.2013.10.051\]\(https://doi.org/10.1016/j.gca.2013.10.051\), 2014.](#)

1691 [Li, L., Bao, C., Sullivan, P. L., Brantley, S., Shi, Y., and Duffy, C.: Understanding watershed](#)
1692 [hydrogeochemistry: 2. Synchronized hydrological and geochemical processes drive stream chemostatic](#)
1693 [behavior, Water Resources Research, 53, 2346-2367, 2017a.](#)

1694 [Li, L., Maher, K., Navarre-Sitchler, A., Druhan, J., Meile, C., Lawrence, C., Moore, J., Perdrial, J., Sullivan, P.,](#)
1695 [Thompson, A., Jin, L., Bolton, E. W., Brantley, S. L., Dietrich, W. E., Mayer, K. U., Steefel, C. I., Valocchi, A.,](#)
1696 [Zachara, J., Kocar, B., McIntosh, J., Tutolo, B. M., Kumar, M., Sonnenthal, E., Bao, C., and Beisman, J.:](#)
1697 [Expanding the role of reactive transport models in critical zone processes, Earth-Science Reviews, 165,](#)
1698 [280-301, <http://dx.doi.org/10.1016/j.earscirev.2016.09.001>, 2017b.](#)

1699 [Li, L.: Watershed reactive transport, Reviews in Mineralogy and Geochemistry, 85, 381-418, 2019.](#)

1700 [Li, L., Sullivan, P. L., Benettin, P., Cirpka, O. A., Bishop, K., Brantley, S. L., Knapp, J. L. A., Meerveld, I.,](#)
1701 [Rinaldo, A., Seibert, J., Wen, H., and Kirchner, J. W.: Toward catchment hydro - biogeochemical theories,](#)
1702 [WIREs Water, \[10.1002/wat2.1495\]\(https://doi.org/10.1002/wat2.1495\), 2020.](#)

1703 [Lin, H.: Temporal stability of soil moisture spatial pattern and subsurface preferential flow pathways in](#)
1704 [the shale hills catchment, Vadose Zone J, 5, 317-340, \[10.2136/vzj2005.0058\]\(https://doi.org/10.2136/vzj2005.0058\), 2006.](#)

1705 [Lindström, G., Rosberg, J., and Arheimer, B.: Parameter Precision in the HBV-NP Model and Impacts on](#)
1706 [Nitrogen Scenario Simulations in the Rönneå River, Southern Sweden, AMBIO: A Journal of the Human](#)
1707 [Environment, 34, 533-537, 535, 2005.](#)

1708 [Lindström, G., Pers, C., Rosberg, J., Strömquist, J., and Arheimer, B.: Development and testing of the HYPE](#)
1709 [\(Hydrological Predictions for the Environment\) water quality model for different spatial scales, Hydrology](#)
1710 [Research, 41, 295-319, \[10.2166/nh.2010.007\]\(https://doi.org/10.2166/nh.2010.007\), 2010.](#)

1711 [Liu, Y., Wang, C., He, N., Wen, X., Gao, Y., Li, S., Niu, S., Butterbach - Bahl, K., Luo, Y., and Yu, G.: A global](#)
1712 [synthesis of the rate and temperature sensitivity of soil nitrogen mineralization: latitudinal patterns and](#)
1713 [mechanisms, Global change biology, 23, 455-464, 2017.](#)

1714 [López, B., Sabaté, S., and Gracia, C.: Vertical distribution of fine root density, length density, area index](#)
1715 [and mean diameter in a Quercus ilex forest, Tree Physiology, 21, 555-560, 2001.](#)

1716 [Maavara, T., Lauerwald, R., Laruelle, G. G., Akbarzadeh, Z., Bouskill, N. J., Van Cappellen, P., and Regnier,](#)
1717 [P.: Nitrous oxide emissions from inland waters: Are IPCC estimates too high?, Global Change Biology, 0,](#)
1718 [doi:10.1111/gcb.14504, 2018.](#)

1719 [Martínez-de la Torre, A., and Miguez-Macho, G.: Groundwater influence on soil moisture memory and](#)
1720 [land-atmosphere fluxes in the Iberian Peninsula, Hydrology and Earth System Sciences, 23, 4909-4932,](#)
1721 [2019.](#)

1722 [Maxwell, R. M., Lundquist, J. K., Mirocha, J. D., Smith, S. G., Woodward, C. S., and Tompson, A. F.:](#)
1723 [Development of a coupled groundwater-atmosphere model, Monthly Weather Review, 139, 96-116,](#)
1724 [2011.](#)

1725 [Mayer, K. U., Frind, E. O., and Blowes, D. W.: Multicomponent reactive transport modeling in variably](#)
1726 [saturated porous media using a generalized formulation for kinetically controlled reactions, Water](#)
1727 [Resources Research, 38, 13-11-13-21, 10.1029/2001wr000862, 2002.](#)

1728 [McMurtrie, R. E., Iversen, C. M., Dewar, R. C., Medlyn, B. E., Näsholm, T., Pepper, D. A., and Norby, R. J.:](#)
1729 [Plant root distributions and nitrogen uptake predicted by a hypothesis of optimal root foraging, Ecology](#)
1730 [and Evolution, 2, 1235-1250, 2012.](#)

1731 [Miller, M. P., Tesoriero, A. J., Hood, K., Terziotti, S., and Wolock, D. M.: Estimating Discharge and Nonpoint](#)
1732 [Source Nitrate Loading to Streams From Three End-Member Pathways Using High-Frequency Water](#)
1733 [Quality Data, Water Resources Research, 53, 10201-10216, 10.1002/2017wr021654, 2017.](#)

1734 [Miller, M. P., Capel, P. D., García, A. M., and Ator, S. W.: Response of Nitrogen Loading to the Chesapeake](#)
1735 [Bay to Source Reduction and Land Use Change Scenarios: A SPARROW - Informed Analysis, JAWRA](#)
1736 [Journal of the American Water Resources Association, 56, 100-112, 2020.](#)

1737 [Moatar, F., Abbott, B. W., Minaudo, C., Curie, F., and Pinay, G.: Elemental properties, hydrology, and](#)
1738 [biology interact to shape concentration - discharge curves for carbon, nutrients, sediment, and major](#)
1739 [ions, Water Resources Research, 53, 1270-1287, 2017.](#)

1740 [Moriasi, D. N., Gowda, P. H., Arnold, J. G., Mulla, D. J., Ale, S., and Steiner, J. L.: Modeling the impact of](#)
1741 [nitrogen fertilizer application and tile drain configuration on nitrate leaching using SWAT, Agricultural](#)
1742 [Water Management, 130, 36-43, https://doi.org/10.1016/j.agwat.2013.08.003, 2013.](#)

1743 [Musolff, A., Schmidt, C., Selle, B., and Fleckenstein, J. H.: Catchment controls on solute export, Adv. Water](#)
1744 [Resour., 86, 133-146, 10.1016/j.advwatres.2015.09.026, 2015.](#)

1745 [Neitsch, S. L., Arnold, J. G., Kiniry, J. R., and Williams, J. R.: Soil and water assessment tool theoretical](#)
1746 [documentation version 2009, Texas Water Resources Institute, 2011.](#)

1747 [Ottoy, S., Elsen, A., Van De Vreken, P., Gobin, A., Merckx, R., Hermy, M., and Van Orshoven, J.: An](#)
1748 [exponential change decline function to estimate soil organic carbon stocks and their changes from topsoil](#)
1749 [measurements, European Journal of Soil Science, 67, 816-826, 2016.](#)

1750 [Porporato, A., D'odorico, P., Laio, F., and Rodriguez-Iturbe, I.: Hydrologic controls on soil carbon and](#)
1751 [nitrogen cycles. I. Modeling scheme, Advances in water resources, 26, 45-58, 2003.](#)

1752 [Qu, Y., and Duffy, C. J.: A semidiscrete finite volume formulation for multiprocess watershed simulation,](#)
1753 [Water Resources Research, 43, W08419, 2007.](#)

1754 [Ranalli, A. J., and Macalady, D. L.: The importance of the riparian zone and in-stream processes in nitrate](#)
1755 [attenuation in undisturbed and agricultural watersheds – A review of the scientific literature, Journal of](#)
1756 [Hydrology, 389, 406-415, https://doi.org/10.1016/j.jhydrol.2010.05.045, 2010.](#)

1757 [Regnier, P., and Steefel, C. I.: A high resolution estimate of the inorganic nitrogen flux from the Scheldt](#)
1758 [estuary to the coastal North Sea during a nitrogen-limited algal bloom, spring 1995, Geochimica et](#)
1759 [Cosmochimica Acta, 63, 1359-1374, 10.1016/s0016-7037\(99\)00034-4, 1999.](#)

1760 [Rutherford, D. W., Chiou, C. T., and Kile, D. E.: Influence of soil organic matter composition on the partition](#)
1761 [of organic compounds, Environmental science & technology, 26, 336-340, 1992.](#)

1762 [Saad, Y., and Schultz, M. H.: GMRES: A generalized minimal residual algorithm for solving nonsymmetric](#)
1763 [linear systems, SIAM Journal on scientific and statistical computing, 7, 856-869, 1986.](#)

1764 [Sabeti, L., Ng, G.-H. C., Nelson, L., Zhi, W., Li, L., La Freniere, J., and Johnstone, M.: Spatiotemporal Drivers](#)
1765 [of Hydrochemical Variability in a Tropical Glacierized Watershed in the Andes, under review.](#)

1766 [Saha, D., Rau, B. M., Kaye, J. P., Montes, F., Adler, P. R., and Kemanian, A. R.: Landscape control of nitrous](#)
1767 [oxide emissions during the transition from conservation reserve program to perennial grasses for](#)
1768 [bioenergy, GCB Bioenergy, 9, 783-795, doi:10.1111/gcbb.12395, 2017.](#)

1769 [Scudeler, C., Pangle, L., Pasetto, D., Niu, G.-Y., Volkmann, T., Paniconi, C., Putti, M., and Troch, P.:](#)
1770 [Multiresponse modeling of variably saturated flow and isotope tracer transport for a hillslope experiment](#)
1771 [at the Landscape Evolution Observatory, Hydrology and Earth System Sciences, 20, 4061-4078, 2016.](#)

1772 [Sebestyen, S. D., Ross, D. S., Shanley, J. B., Elliott, E. M., Kendall, C., Campbell, J. L., Dail, D. B., Fernandez,](#)
1773 [I. J., Goodale, C. L., and Lawrence, G. B.: Unprocessed Atmospheric Nitrate in Waters of the Northern](#)
1774 [Forest Region in the US and Canada, Environmental science & technology, 53, 3620-3633, 2019.](#)

1775 [Seibert, J., Grabs, T., Köhler, S., Laudon, H., Winterdahl, M., and Bishop, K.: Linking soil- and stream-water](#)
1776 [chemistry based on a Riparian Flow-Concentration Integration Model, Hydrol. Earth Syst. Sci., 13, 2287-](#)
1777 [2297, 10.5194/hess-13-2287-2009, 2009.](#)

1778 [Seyfried, M., Lohse, K., Marks, D., Flerchinger, G., Pierson, F., and Holbrook, W. S.: Reynolds Creek](#)
1779 [Experimental Watershed and Critical Zone Observatory, Vadose Zone Journal, 17, 180129,](#)
1780 [10.2136/vzj2018.07.0129, 2018.](#)

1781 [Shi, Y.: Development of a land surface hydrologic modeling and data assimilation system for the study of](#)
1782 [subsurface-land surface interaction, 2012.](#)

1783 [Shi, Y., Davis, K. J., Duffy, C. J., and Yu, X.: Development of a coupled land surface hydrologic model and](#)
1784 [evaluation at a critical zone observatory, Journal of Hydrometeorology, 14, 1401-1420, 2013.](#)

1785 [Shi, Y., Eissenstat, D. M., He, Y., and Davis, K. J.: Using a spatially-distributed hydrologic biogeochemistry](#)
1786 [model with a nitrogen transport module to study the spatial variation of carbon processes in a Critical](#)
1787 [Zone Observatory, Ecological Modelling, 380, 8-21, 2018.](#)

1788 [Skamarock, W., and Klemp, J.: A Description of the Advanced Research WRF Model Version 4. Ncar](#)
1789 [Technical Notes, No, NCAR/TN-556+ STR, 2019.](#)

1790 [Song, X., Zhang, J., Zhan, C., Xuan, Y., Ye, M., and Xu, C.: Global sensitivity analysis in hydrological modeling:](#)
1791 [Review of concepts, methods, theoretical framework, and applications, Journal of hydrology, 523, 739-](#)
1792 [757, 2015.](#)

1793 [Steeffel, C., Appelo, C., Arora, B., Jacques, D., Kalbacher, T., Kolditz, O., Lagneau, V., Lichtner, P., Mayer, K.](#)
1794 [U., and Meeussen, J.: Reactive transport codes for subsurface environmental simulation, Computational](#)
1795 [Geosciences, 19, 445-478, 2015.](#)

1796 [Steeffel, C. I., and Lasaga, A. C.: A coupled model for transport of multiple chemical species and kinetic](#)
1797 [precipitation/dissolution reactions with application to reactive flow in single phase hydrothermal systems,](#)
1798 [American Journal of science, 294, 529-592, 1994.](#)

1799 [Steimke, A. L., Han, B., Brandt, J. S., and Flores, A. N.: Climate change and curtailment: Evaluating water](#)
1800 [management practices in the context of changing runoff regimes in a snowmelt-dominated basin, Water,](#)
1801 [10, 1490, 2018.](#)

1802 [Sullivan, P. L., Hynek, S. A., Gu, X., Singha, K., White, T., West, N., Kim, H., Clarke, B., Kirby, E., Duffy, C.,](#)
1803 [and Brantley, S. L.: Oxidative dissolution under the channel leads geomorphological evolution at the Shale](#)
1804 [Hills catchment, American Journal of Science, 316, 981-1026, 10.2475/10.2016.02, 2016.](#)

1805 [Suseela, V., Conant, R. T., Wallenstein, M. D., and Dukes, J. S.: Effects of soil moisture on the temperature](#)
1806 [sensitivity of heterotrophic respiration vary seasonally in an old - field climate change experiment, Global](#)
1807 [Change Biology, 18, 336-348, 2012.](#)

1808 [Taylor, R. G., Scanlon, B., Döll, P., Rodell, M., Van Beek, R., Wada, Y., Longuevergne, L., Leblanc, M.,](#)
1809 [Famiglietti, J. S., and Edmunds, M.: Ground water and climate change, *Nature climate change*, 3, 322,](#)
1810 [2013.](#)

1811 [Todd, D. K., and Mays, L. W.: *Groundwater Hydrology*, Welly Inte, 2005.](#)

1812 [van der Velde, Y., de Rooij, G. H., Rozemeijer, J. C., van Geer, F. C., and Broers, H. P.: Nitrate response of](#)
1813 [a lowland catchment: On the relation between stream concentration and travel time distribution](#)
1814 [dynamics, *Water Resources Research*, 46, 10.1029/2010wr009105, 2010.](#)

1815 [van der Velde, Y., Vercauteren, N., Jaramillo, F., Dekker, S. C., Destouni, G., and Lyon, S. W.: Exploring](#)
1816 [hydroclimatic change disparity via the Budyko framework, *Hydrological Processes*, 28, 4110-4118,](#)
1817 [10.1002/hyp.9949, 2014.](#)

1818 [Weiler, M., and McDonnell, J. R. J.: Testing nutrient flushing hypotheses at the hillslope scale: A virtual](#)
1819 [experiment approach, *J. Hydrol.*, 319, 339-356, 10.1016/j.jhydrol.2005.06.040, 2006.](#)

1820 [Weitzman, J. N., and Kaye, J. P.: Nitrogen Budget and Topographic Controls on Nitrous Oxide in a Shale -](#)
1821 [Based Watershed, *Journal of Geophysical Research: Biogeosciences*, 123, 1888-1908, 2018.](#)

1822 [Wen, H., Perdrial, J., Bernal, S., Abbott, B. W., Dupas, R., Godsey, S. E., Harpold, A., Rizzo, D., Underwood,](#)
1823 [K., and Adler, T.: Temperature controls production but hydrology controls export of dissolved organic](#)
1824 [carbon at the catchment scale, 24, 945-966, 2020.](#)

1825 [Wieder, W. R., Allison, S. D., Davidson, E. A., Georgiou, K., Hararuk, O., He, Y., Hopkins, F., Luo, Y., Smith,](#)
1826 [M. J., and Sulman, B.: Explicitly representing soil microbial processes in Earth system models, *Global*](#)
1827 [Biogeochemical Cycles, 29, 1782-1800, 2015.](#)

1828 [Winter, T., Harvey, J., Franke, O., and Alley, W.: Natural processes of ground-water and surface-water](#)
1829 [interaction, *Ground Water and Surface Water: A Single Resource*, US Geological Survey Circular, 1139, 2-](#)
1830 [50, 1998.](#)

1831 [Wolery, T. J.: EQ3/6, a software package for geochemical modeling of aqueous systems: package overview](#)
1832 [and installation guide \(version 7.0\), 1992.](#)

1833 [Xiao, D., Shi, Y., Brantley, S. L., Forsythe, B., DiBiase, R., Davis, K., and Li, L.: Streamflow Generation From](#)
1834 [Catchments of Contrasting Lithologies: The Role of Soil Properties, Topography, and Catchment Size,](#)
1835 [Water Resources Research, n/a, 10.1029/2018wr023736, 2019.](#)

1836 [Yan, Q., Duan, Z., Mao, J., Li, X., and Dong, F.: Effects of root-zone temperature and N, P, and K supplies](#)
1837 [on nutrient uptake of cucumber \(*Cucumis sativus* L.\) seedlings in hydroponics, *Soil Science and Plant*](#)
1838 [Nutrition, 58, 707-717, 2012.](#)

1839 [Yan, Z., Bond-Lamberty, B., Todd-Brown, K. E., Bailey, V. L., Li, S., Liu, C., and Liu, C.: A moisture function](#)
1840 [of soil heterotrophic respiration that incorporates microscale processes, *Nat Commun*, 9, 2562,](#)
1841 [10.1038/s41467-018-04971-6, 2018.](#)

1842 [Zarnetske, J. P., Bouda, M., Abbott, B. W., Saiers, J., and Raymond, P. A.: Generality of hydrologic transport](#)
1843 [limitation of watershed organic carbon flux across ecoregions of the United States, *Geophysical Research*](#)
1844 [Letters, 45, 11,702-711,711, 2018.](#)

1845 [Zhi, W., Li, L., Dong, W., Brown, W., Kaye, J., Steefel, C., and Williams, K. H.: Distinct Source Water](#)
1846 [Chemistry Shapes Contrasting Concentration-Discharge Patterns, *Water Resources Research*, 55, 4233-](#)
1847 [4251, 10.1029/2018wr024257, 2019.](#)

1848 [Zhi, W., and Li, L.: The Shallow and Deep Hypothesis: Subsurface Vertical Chemical Contrasts Shape Nitrate](#)
1849 [Export Patterns from Different Land Uses, *Environmental Science & Technology*, 54, 11915-11928,](#)
1850 [10.1021/acs.est.0c01340, 2020.](#)

1851 [Zhi, W., Williams, K. H., Carroll, R. W. H., Brown, W., Dong, W., Kerins, D., and Li, L.: Significant stream](#)
1852 [chemistry response to temperature variations in a high-elevation mountain watershed, *Communications*](#)
1853 [Earth & Environment, 1, 10.1038/s43247-020-00039-w, 2020.](#)

1854 [Zhou, T., Shi, P., Hui, D., and Luo, Y.: Global pattern of temperature sensitivity of soil heterotrophic](#)
1855 [respiration \(Q10\) and its implications for carbon - climate feedback, Journal of Geophysical Research:](#)
1856 [Biogeosciences, 114, 2009.](#)

1857

1858

1859